Multiscale analysis of composite structures based on higher-order asymptotic homogenization with boundary layer correction

Mouad Fergoug, Augustin Parret-Fréaud, Nicolas Feld, Basile Marchand, Samuel Forest

Multiscale analysis of composite structures based on higher-order asymptotic homogenization with boundary layer correction

Mouad Fergoug[1,2*], Augustin Parret-Fréaud[1], Nicolas Feld[1], Basile Marchand[2], Samuel Forest[2]

[1] *Safran Tech, Etablissement Paris Saclay, rue des Jeunes Bois-Châteaufort, 78114 Magny-les-Hameaux, France*

[2] *MINES Paris, PSL University, MAT – Centre des matériaux, CNRS UMR 7633, BP 87 91003 Evry, France*

https://doi.org/10.1016/j.euromechsol.2022.104754

Abstract

First-order homogenization generally becomes inaccurate for materials with a weak scale separation between characteristic lengths of the heterogeneities and the structural problem. It is also unable to provide a correct solution in the vicinity of the boundaries due to the loss of periodicity in these regions. In this article, we demonstrate the effectiveness of higher-order homogenization, up to the third-order, in estimating correctly the heterogeneous solution, for cases with a low scale separation in elastic composite materials. We also propose a higher-order general boundary layer method, effective for various boundary conditions (Dirichlet, Neumann or mixed), to correct the obtained estimation near the boundaries. The efficiency and accuracy of the proposed methods are studied on various numerical examples dealing with elastic laminates and fiber-matrix composites.

Keywords: asymptotic homogenization, periodic materials, boundary layer effect.

[*]Corresponding author

Email address: mouad.fergoug@mines-paristech.fr (Mouad Fergoug[1,2])

1. Introduction

Classical or first-order homogenization methods assume a complete separation of scales in composite materials. This assumption is only valid when the scale of the microstructure or microstructural fluctuation is much smaller than the characteristic dimension of the macrostructure. Most of these homogenization methods are known to be effective in capturing uniform macroscopic strain fields without large gradients. For weak separation of scales, however, they generally become inaccurate (Ameen et al., 2018). Such cases can occur mainly when: (a) The size of the microstructure is of the same order of magnitude as that of the macrostructure, and (b) the wave length of variation of macroscale fields is not sufficiently large compared to the size of the microstructure. In such cases, the predicted properties obtained by first-order homogenization may fail to describe the local or global responses of the composite (Ameen et al., 2018; Kouznetsova et al., 2002; He and Pindera, 2020a). This is mainly explained by two reasons:

- The scale separation assumption implicitly implies macroscopic quasi-uniformity of the strain field over the microstructure. Therefore, only first-order deformation modes (tension, compression, and shear) are considered. In contrast, in the case of weak separation of scales, capturing a bending mode, for example, remains beyond the capabilities of classical homogenization (Kouznetsova et al., 2002; Fergoug et al., 2022), as will be shown later in this article.

- Higher-order homogenization may require consideration of non-local media. Indeed, classical homogenization methods take into account the influence of the volume fraction, distribution and morphology of the microstructure (Sanchez-

Palencia and Zaoui, 1987; Suquet, 2014), but cannot account for geometrical size effects in the mechanical behavior of heterogeneous materials.

To overcome these limitations, generalized continuum theories (higher-order continua or higher-grade theories) are used to describe the behavior of either the microscopic scale or the macroscopic one, or both levels simultaneously. Indeed, enriched continuum theories extend the range of applicability of homogenization methods beyond the strict assumption of scale separation. They also enable a relaxation of the local action principle by introducing some additional length scale parameters to take into account the influence of the surrounding physical state on the behavior of a continuum point.

Two main categories of generalized continua are distinguished:

- Higher-order continua that introduce additional degrees of freedom, like the Cosserat medium proposed by the Cosserat brothers (Cosserat and Cosserat, 1909) where local micro-rotations are introduced at each continuum point in addition to the displacement field. This enhancement can be extended further to obtain the micromorphic elasticity (Mindlin, 1964; Germain, 1973).

- Higher-grade continua according to Mindlin (1964); Mindlin and Eshel (1968) that include higher-order gradients of kinematic or internal variables in the expression of the (elastic) energy density.

The strain-gradient continuum offers some advantages compared to higher-order continua as stated in Yvonnet et al. (2020). Indeed, this model is rich enough to incorporate a characteristic length of the microstructure without introducing a large number of parameters as in micromorphic elasticity (Auffray et al., 2015). Furthermore, such a model can be constructed by asymptotic analyses (Boutin, 1996; Smyshlyaev and

Cherednichenko, 2000; Peerlings and Fleck, 2004; Tran et al., 2012).

In most cases, it is agreed that including higher gradients of the macroscopic field in the homogenization of a Representative Volume Element (RVE) is a natural way to introduce the internal length scale characterizing the microstructure. At least two approaches exist regarding this subject.

The first approach uses Quadratic Boundary Conditions (QBCs) applied to the unit-cell (Gologanu et al., 1997; Forest, 1998; Forest et al., 2001; Kouznetsova et al., 2002; Yvonnet et al., 2020). This method is an extension of the classical Kinematic Uniform Boundary Conditions (KUBC) (Huet, 1990; Kanit et al., 2003) which consist in applying, on the boundary of the RVE, the displacement field that would occur if the strain field was uniform. Indeed, a displacement that has a quadratic dependence with the position vector is applied, with the macroscopic gradient of strain being the considered enforcing term. This method has a major flaw: QBCs lead to non-zero fluctuations when the material is homogeneous, which seems to be physically unreasonable as stated by Yuan et al. (2008), Forest and Trinh (2011), Tran et al. (2012), Monchiet et al. (2020), and Yvonnet et al. (2020), since these fluctuations are due to the heterogeneity of the microstructure. To tackle this, a correction has been proposed in Monchiet et al. (2020) by adding adequate body forces to QBCs and has been successfully used in Yvonnet et al. (2020).

The second approach considers higher-order problems in the asymptotic homogenization method. This approach of series expansion, initially presented by Sanchez-Palencia (1983); Bensoussan et al. (2011) for periodic heterogeneous materials, introduces a scale factor $\epsilon = l/L$, where l and L are the characteristic lengths of the microstructure and macrostructure, respectively. In the case of a strict scale separation, *i.e.* $\epsilon \ll 1$, classical homogenization gives adequate estimate properties. In cases of weak scale separation, *i.e.* $\epsilon < 1$, the solution can be approximated by

keeping higher-order terms in the series expansion. These terms are obtained by resolving a hierarchical set of elasticity problems with prescribed body forces and eigenstrains, obtained from the solution at the lower-order. It is shown in Boutin (1996) that higher-order terms in asymptotic homogenization introduce successive gradients of macroscale strain and tensors characteristic of the microstructure, which result in introducing a non-local effect in the material behavior. The analytical solutions of these characteristic tensors were provided by Boutin (1996) for a laminate. The agreement with the phenomenological strain-gradient theories was established by Smyshlyaev and Cherednichenko (2000); Peerlings and Fleck (2004); Tran et al. (2012) by combining the asymptotic method with a variational technique.

In the present paper, the retained method for our multiscale analyses is the asymptotic homogenization method. Consequently, only periodic heterogeneous materials are considered where the period, *i.e.* the unit-cell, defines the RVE without any ambiguity.

We establish a general numerical framework to evaluate the effect of macroscopic strain gradients on the local response of the composite. This framework is implemented, in this article, using the Finite Element Method (FEM) but could be implemented by using another discretization method. We perform a relocalization process to estimate heterogeneous local fields by considering higher-order homogenization problems, up to the third-order in the asymptotic expansion. This relocalization process is associated with a macroscale problem, which remains, in this work, a scale-independent Cauchy type. Our numerical implementation of the localization tensors will be verified based on analytical solutions provided by Boutin (1996) (see appendix A).

While asymptotic homogenization may estimate local fields within the composite by a relocalization process, the construction of a solution at the vicinity of the bound-

aries remains beyond the capabilities of classical homogenization (Sanchez-Palencia, 1986; Dumontet, 1986; Koley et al., 2019; Fergoug et al., 2022). Indeed, asymptotic homogenization assumes a periodic solution, which is not the case on the boundaries. It has been shown by Pipes et al. (1973); Tang and Levy (1975); Hsu and Herakovich (1977); Pagano (1978) that complex stress states with a rapid change of gradients occur within a local region near the boundaries, frequently referred to as a *boundary layer effect*. This effect is often responsible for the initiation of structural failure, *e.g.* in laminates (Pipes et al., 1973).

In a previous work (Fergoug et al., 2022), a general boundary layer correction was proposed. It is valid for different Boundary Conditions (BCs): Dirichlet, Neumann or mixed. The main idea of this method is to enrich, on boundaries, the first-order relocalized solution fields by adding decaying corrective terms obtained by the resolution of independent auxiliary problems over the unit-cell. The nature of the problems to be solved depends on the actual boundary conditions applied locally to the structure. These corrective terms are then added to the first-order relocalized fields.

In the present article, we propose an extension of this general boundary layer correction to rectify higher-order relocalization fields up to the third-order. Indeed, matching boundary conditions requires the introduction of boundary layers at each order.

Regarding the aforementioned aspects, the present work proposes two main aspects:

- A higher-order relocalization process up to the third-order. This means that we the introduce effects of the macroscopic strain, its gradient, and its second gradient on the local response of the composite. By doing so, we extend the range of applicability of relocalization to cases subjected where a first-order homogenization/relocalization is generally not valid anymore.

- A general boundary layer correction to accurately estimate higher-order relocalized fields, up to the third-order, on the boundaries.

To the best knowledge of the authors, such an extension of first-order boundary layer correction has not been yet proposed in the literature.

A computing workflow is proposed to perform both the relocalization step and the boundary layer correction within a finite element framework.

The outline of the paper is as follows. In Sec. 2, we first briefly recall the asymptotic expansion homogenization method and describe the proposed higher-order relocalization process. In Sec. 3, we detail the proposed general boundary layer correction procedure. A numerical implementation procedure is proposed in Sec. 4. Numerical examples are presented and discussed in Sec. 5, with the objective of demonstrating the efficiency of the suggested approach.

2. Higher-order estimation of micromechanical fields

Conventionally in mechanical homogenization, asymptotic series are truncated at the first-order. It follows that the obtained effective macroscopic continuum is a scale-independent Cauchy type continuum. The consequence of taking into account additional terms of the expansion, up to the third-order, as derived by Boutin (1996), is to introduce scale-dependent corrective terms in the material behavior.

The objective of this section is to describe the proposed estimation of local heterogeneous fields based on a higher-order relocalization process. This relocalization stage is associated with a given macroscale equilibrium state also elaborated in this section.

2.1. Statement of the boundary value problem and homogenization procedure

Consider a problem domain Ω^ϵ, formed by the spatial repetition of a heterogeneous unit-cell, as shown in Fig. 1. This body, considered as a linear elastic solid

in static equilibrium, is subjected to a body force $\boldsymbol{f}$ per unit volume. The boundary $\partial\Omega^\epsilon$ consists of a portion Γ_u, on which the displacements are prescribed to the value $\boldsymbol{u}^d$, and a portion Γ_t on which surface traction $\boldsymbol{F}^d$ per unit area are prescribed, such that $\partial\Omega^\epsilon = \Gamma_u \cup \Gamma_t$, and $\Gamma_u \cap \Gamma_t = \emptyset$.
Because of the heterogeneous nature of the material, the corresponding mechanical behavior depends on two scales:

- Macroscale with domain Ω, free of heterogeneities, having L as a characteristic length and global coordinates $\boldsymbol{x} \in \Omega$ with the assumption that $\partial\Omega^\epsilon = \partial\Omega$ (see Fig. 1).

- Microscale, having l as a characteristic length and with local coordinates $\boldsymbol{y} \in Y$, where Y is the unit-cell domain, typically chosen here to be an open rectangular parallelepiped $Y =]0, Y_1[\times]0, Y_2[\times]0, Y_3[$ (see Fig. 1).

The coarse and fine scales are related by the parameter ϵ such that:

$$\epsilon = \frac{l}{L}, \qquad \boldsymbol{y} = \frac{\boldsymbol{x}}{\epsilon}. \tag{1}$$

The domain Ω^ϵ can be considered as the product space $\Omega \times Y$:

$$\Omega^\epsilon = \left\{ \boldsymbol{x} \in \Omega \middle| \left(\boldsymbol{y} = \frac{\boldsymbol{x}}{\epsilon} \right) \in Y \right\}. \tag{2}$$

Since the heterogeneity of the material arises from the periodically repeating unit-cell, and owing to this periodicity, one can define the elasticity tensor $\mathbb{C}$ as $Y-$periodic:

$$\mathbb{C} = \mathbb{C}\left(\boldsymbol{y}\right). \tag{3}$$

The heterogeneous stiffness tensor reads $\mathbb{C}^\epsilon\left(\boldsymbol{x}\right) = \mathbb{C}\left(\boldsymbol{x}/\epsilon\right) = \mathbb{C}\left(\boldsymbol{y}\right)$, the superscript indicating fine-scale dependence. Similarly, the microscale displacement, strain, and

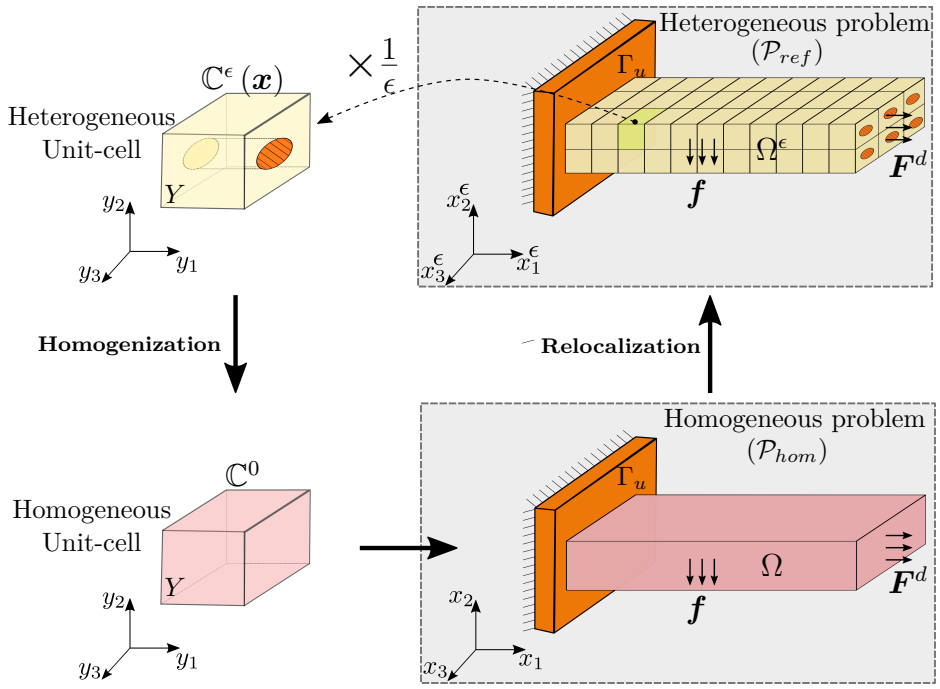

Figure 1: Illustration (Fergoug et al., 2022) of the heterogeneous problem $(\mathcal{P}_{ref})$ with domain Ω^ϵ, constructed by translating the unit-cell Y characterized by an oscillatory behavior $\mathbb{C}^\epsilon(\boldsymbol{x})$ over the three space directions. The homogenized problem $(\mathcal{P}_{hom})$ with homogeneous domain Ω is characterized by the homogenized elasticity tensor $\mathbb{C}^0$ obtained from the homogenization step. Microscale fields are estimated by a relocalization process.

stress fields read $\boldsymbol{u}^\epsilon$, $\boldsymbol{\varepsilon}^\epsilon$, and $\boldsymbol{\sigma}^\epsilon$, respectively.

In our previous work (Fergoug et al., 2022), we have defined the following boundary value problems:

- Heterogeneous problem $(\mathcal{P}_{ref})$ with solution $(\boldsymbol{u}^\epsilon, \boldsymbol{\varepsilon}^\epsilon, \boldsymbol{\sigma}^\epsilon)$. This problem is usually intractable by Direct Numerical Simulation (DNS, *i.e.* when the geometry of the microstructure is explicitly described in simulations). Common practice would call for a tractable estimate.

- First-order periodic problem $\left(\mathcal{P}_{order}^{1^{st}}\right)$ used to deduce the homogenized elasticity tensor $\mathbb{C}^0$ and first-order displacement, strain, and stress localization tensors: $\mathbb{D}^0$, $\mathbb{A}^0$, and $\mathbb{B}^0$, respectively.

- Homogenized problem $(\mathcal{P}_{hom})$ corresponding to the macroscale with solution (displacement $\boldsymbol{U}$, strain $\boldsymbol{E}$, stress $\boldsymbol{\Sigma}$), characterized by the homogenized elasticity tensor $\mathbb{C}^0$.

Formal definitions of these problems are omitted here for conciseness; we refer the reader to Fergoug et al. (2022) for more details.

We aim to truncate the asymptotic expansion up to the third-order. Therefore, mechanical fields, solution to $(\mathcal{P}_{ref})$, are approximated with an asymptotic expansion in powers of the small parameter ϵ as:

$$\boldsymbol{u}^{\epsilon}(\boldsymbol{x}) = \boldsymbol{u}^{0}(\boldsymbol{x},\boldsymbol{y}) + \epsilon\boldsymbol{u}^{1}(\boldsymbol{x},\boldsymbol{y}) + \epsilon^{2}\boldsymbol{u}^{2}(\boldsymbol{x},\boldsymbol{y}) + \epsilon^{3}\boldsymbol{u}^{3}(\boldsymbol{x},\boldsymbol{y}) + \mathcal{O}\left(\epsilon^{4}\right), \tag{4}$$

$$\boldsymbol{\varepsilon}^{\epsilon}(\boldsymbol{x}) = \boldsymbol{\varepsilon}^{0}(\boldsymbol{x},\boldsymbol{y}) + \epsilon\boldsymbol{\varepsilon}^{1}(\boldsymbol{x},\boldsymbol{y}) + \epsilon^{2}\boldsymbol{\varepsilon}^{2}(\boldsymbol{x},\boldsymbol{y}) + \mathcal{O}\left(\epsilon^{3}\right), \tag{5}$$

$$\boldsymbol{\sigma}^{\epsilon}(\boldsymbol{x}) = \boldsymbol{\sigma}^{0}(\boldsymbol{x},\boldsymbol{y}) + \epsilon\boldsymbol{\sigma}^{1}(\boldsymbol{x},\boldsymbol{y}) + \epsilon^{2}\boldsymbol{\sigma}^{2}(\boldsymbol{x},\boldsymbol{y}) + \mathcal{O}\left(\epsilon^{3}\right). \tag{6}$$

The quantities $\boldsymbol{u}^n$, $\boldsymbol{\varepsilon}^n$ and $\boldsymbol{\sigma}^n$ are $Y-$periodic functions called *correctors* of the displacement, strain, and stress fields, respectively.

The following formulation for higher-order homogenization is classical without new developments. Nevertheless, efforts have been made to detail formulation of hierarchical periodic problems, up to the third-order. Details of the prescribed body forces and eigenstrains, used to solve these periodic problems, are provided. Furthermore, since our objective is to conduct a higher-order relocalization process, the localization tensors at different orders are also provided.

Second-order periodic problem $\left(\mathcal{P}^{2^{nd}}_{order}\right)$

This problem is defined on the unit-cell Y. Its solution are the displacement corrector $\boldsymbol{u}^2$ and stress $\boldsymbol{\sigma}^1$. It reads:

Find $(\boldsymbol{u}^2, \boldsymbol{\sigma}^1)$ such that:

$$\left(\mathcal{P}^{2^{nd}}_{order}\right): \begin{cases} \operatorname{div}_y\left(\boldsymbol{\sigma}^1(\boldsymbol{x},\boldsymbol{y})\right) + \boldsymbol{L}^1(\boldsymbol{x},\boldsymbol{y}) = 0, & \forall \boldsymbol{y} \in Y, \quad (7a) \\ \boldsymbol{\sigma}^1(\boldsymbol{x},\boldsymbol{y}) = \mathbb{C}(\boldsymbol{y}) : \left(\boldsymbol{\varepsilon}_y(\boldsymbol{u}^2) + \boldsymbol{\eta}^1(\boldsymbol{x},\boldsymbol{y})\right), & \forall \boldsymbol{y} \in Y, \quad (7b) \\ \boldsymbol{u}^2(\boldsymbol{x},\boldsymbol{y}) \quad \text{is } Y-\text{periodic}, & (7c) \\ \boldsymbol{\sigma}^1(\boldsymbol{x},\boldsymbol{y}) \cdot \boldsymbol{n} \quad \text{is } Y-\text{antiperiodic}, & (7d) \end{cases}$$

with:

$$\boldsymbol{\varepsilon}_y(\boldsymbol{u}^2) = \operatorname{sym}\left(\nabla_y \boldsymbol{u}^2\right) = \frac{1}{2}\left(\nabla_y \boldsymbol{u}^2 + \left(\nabla_y \boldsymbol{u}^2\right)^\top\right). \tag{8}$$

The body force $\boldsymbol{L}^1(\boldsymbol{x},\boldsymbol{y})$ and the strain field $\boldsymbol{\eta}^1(\boldsymbol{x},\boldsymbol{y})$ read:

$$\begin{cases} \boldsymbol{L}^1(\boldsymbol{x},\boldsymbol{y}) = \left(\mathbb{B}^0(\boldsymbol{y}) - \left\langle \mathbb{B}^0(\boldsymbol{y}) \right\rangle_Y\right) \vdots \boldsymbol{\nabla}_x \boldsymbol{E}(\boldsymbol{x}), \\ \boldsymbol{\eta}^1(\boldsymbol{x},\boldsymbol{y}) = \operatorname{sym}\left(\mathbb{D}^0(\boldsymbol{y}) : \boldsymbol{\nabla}_x \boldsymbol{E}(\boldsymbol{x})\right). \end{cases} \tag{9}$$

The periodic fluctuation $\boldsymbol{u}^2$ takes the following form:

$$\boldsymbol{u}^2(\boldsymbol{x},\boldsymbol{y}) = \mathbb{D}^1(\boldsymbol{y}) \vdots \boldsymbol{\nabla}_x \boldsymbol{E}(\boldsymbol{x}), \tag{10}$$

where $\mathbb{D}^1(\boldsymbol{y})$ is a fourth-rank tensor, called second-order displacement localization tensor. It is periodic over unit-cell Y and verifies $\langle \mathbb{D}^1 \rangle_Y = 0$, where $\langle \bullet \rangle_Y = \frac{1}{|Y|}\int_Y \bullet \, dY$ indicates the volume average over unit-cell Y.

The second-order strain corrector reads:

$$\boldsymbol{\varepsilon}^1(\boldsymbol{x},\boldsymbol{y}) = \mathbb{A}^1(\boldsymbol{y}) \vdots \boldsymbol{\nabla}_x \boldsymbol{E}(\boldsymbol{x}), \tag{11}$$

where $\mathbb{A}^1(\boldsymbol{y})$ is a fifth-rank tensor, called second-order strain localization tensor. We therefore can define the second-order stress corrector as:

$$\boldsymbol{\sigma}^1(\boldsymbol{x},\boldsymbol{y}) = \mathbb{C}(\boldsymbol{y}) : \boldsymbol{\varepsilon}^1(\boldsymbol{x},\boldsymbol{y}) = \mathbb{B}^1(\boldsymbol{y}) \vdots \boldsymbol{\nabla}_x \boldsymbol{E}(\boldsymbol{x}), \tag{12}$$

where

$$\mathbb{B}^1(\boldsymbol{y}) = \mathbb{C}(\boldsymbol{y}) : \mathbb{A}^1(\boldsymbol{y}), \tag{13}$$

is the fifth-rank stress localization tensor.

The effective, fifth-rank, elasticity tensor $\mathbb{C}^1$, which depends on the microstructure, is deduced from the volume average of the stress localization tensor over the unit-cell:

$$\mathbb{C}^1 = \left\langle \mathbb{B}^1(\boldsymbol{y}) \right\rangle_Y. \tag{14}$$

The tensor $\mathbb{C}^1$ is of odd rank and therefore equals to *zero* in case of centro-symmetric unit-cell.

Third-order periodic problem $\left(\mathcal{P}^{3rd}_{order}\right)$

This problem is defined on the unit-cell Y. Its solution are the displacement corrector $\boldsymbol{u}^3$ and stress $\boldsymbol{\sigma}^2$. It reads:

Find $(\boldsymbol{u}^3, \boldsymbol{\sigma}^2)$ such that:

$$\left(\mathcal{P}^{3rd}_{order}\right) : \begin{cases} \operatorname{div}_y\left(\boldsymbol{\sigma}^2(\boldsymbol{x},\boldsymbol{y})\right) + \boldsymbol{L}^2(\boldsymbol{x},\boldsymbol{y}) = 0, & \forall \boldsymbol{y} \in Y, \quad (15a) \\ \boldsymbol{\sigma}^2(\boldsymbol{x},\boldsymbol{y}) = \mathbb{C}(\boldsymbol{y}) : \left(\boldsymbol{\varepsilon}_y(\boldsymbol{u}^3) + \boldsymbol{\eta}^2(\boldsymbol{x},\boldsymbol{y})\right), & \forall \boldsymbol{y} \in Y, \quad (15b) \\ \boldsymbol{u}^3(\boldsymbol{x},\boldsymbol{y}) \quad \text{is } Y-\text{periodic}, & (15c) \\ \boldsymbol{\sigma}^2(\boldsymbol{x},\boldsymbol{y}) \cdot \boldsymbol{n} \quad \text{is } Y-\text{antiperiodic}. & (15d) \end{cases}$$

The body force $\boldsymbol{L}^2(\boldsymbol{x},\boldsymbol{y})$ and the strain field $\boldsymbol{\eta}^2(\boldsymbol{x},\boldsymbol{y})$ read:

$$\begin{cases} \boldsymbol{L}^2(\boldsymbol{x},\boldsymbol{y}) = \left(\mathbb{B}^1(\boldsymbol{y}) - \left\langle \mathbb{B}^1(\boldsymbol{y}) \right\rangle_Y\right) \;::\; \boldsymbol{\nabla}_x\boldsymbol{\nabla}_x\boldsymbol{E}(\boldsymbol{x}), \\ \boldsymbol{\eta}^2(\boldsymbol{x},\boldsymbol{y}) = \mathrm{sym}\left(\mathbb{D}^1(\boldsymbol{y}) \;\vdots\; \boldsymbol{\nabla}_x\boldsymbol{\nabla}_x\boldsymbol{E}(\boldsymbol{x})\right). \end{cases} \tag{16}$$

Similarly to the second-order, a body force and eigenstrain based on the solution to the previous order are prescribed over the unit-cell.

The periodic fluctuation $\boldsymbol{u}^3$, solution to the third-order problem, reads:

$$\boldsymbol{u}^3(\boldsymbol{x},\boldsymbol{y}) = \mathbb{D}^2(\boldsymbol{y}) :: \boldsymbol{\nabla}_x\boldsymbol{\nabla}_x\boldsymbol{E}(\boldsymbol{x}), \tag{17}$$

where $\mathbb{D}^2(\boldsymbol{y})$ is a fifth-rank tensor, called third-order displacement localization tensor. It is periodic over unit-cell Y and verifies $\langle \mathbb{D}^2 \rangle_Y = 0$.

The third-order strain corrector reads:

$$\boldsymbol{\varepsilon}^2(\boldsymbol{x},\boldsymbol{y}) = \mathbb{A}^2(\boldsymbol{y}) :: \boldsymbol{\nabla}_x\boldsymbol{\nabla}_x\boldsymbol{E}(\boldsymbol{x}), \tag{18}$$

where $\mathbb{A}^2(\boldsymbol{y})$ is a sixth-rank tensor, called third-order strain localization tensor. We can therefore define the third-order stress corrector as:

$$\boldsymbol{\sigma}^2(\boldsymbol{x},\boldsymbol{y}) = \mathbb{C}(\boldsymbol{y}) : \boldsymbol{\varepsilon}^2(\boldsymbol{x},\boldsymbol{y}) = \mathbb{B}^2(\boldsymbol{y}) :: \boldsymbol{\nabla}_x\boldsymbol{\nabla}_x\boldsymbol{E}(\boldsymbol{x}), \tag{19}$$

where

$$\mathbb{B}^2(\boldsymbol{y}) = \mathbb{C}(\boldsymbol{y}) : \mathbb{A}^2(\boldsymbol{y}), \tag{20}$$

is the third-rank stress localization tensor.

The effective, sixth-rank, elasticity tensor $\mathbb{C}^2$ reads:

$$\mathbb{C}^2 = \left\langle \mathbb{B}^2(\boldsymbol{y}) \right\rangle_Y. \tag{21}$$

For both second and third-order problems, the applied body forces and eigenstrains are related to successive gradients of the macroscopic strain tensor. Hence, the

resolution of these problems introduces a non-local effect in the material behavior. When strain gradients are significant, contributions of higher-order correctors become significant as well. In contrast, a weaker contribution is expected for quasi-homogeneous deformation cases. For these reasons, the possible drawback of QBCs approaches highlighted in the introduction, that strain gradient effects persist even when the material is homogeneous, does not concern periodic homogenization based on asymptotic series expansion.

2.2. Proposed micromechanical fields estimates

Fergoug et al. (2022) have shown that a first-order relocalization may provide an accurate estimate of DNS fields, provided that macroscale strain gradients remain sufficiently small. Indeed, for a bending case, it was shown that the first-order estimate may not be accurate anymore (Fergoug et al., 2022).
We propose a better estimate of DNS fields by conducting a higher-order relocalization process which takes into account additional terms of the asymptotic expansion, up to the third-order. This is expected to capture the effect of macroscopic successive gradients, and thus introduce a length scale in the modeling.
This estimate is built here using:

- The macroscale strain and its successive gradients obtained from the resolution of the homogeneous problem ($\mathcal{P}_{hom}$). We recall that the homogenized macroscopic continuum is a scale-independent Cauchy type.
- localization tensors $(\mathbb{D}^0, \mathbb{A}^0, \mathbb{B}^0)$, $(\mathbb{D}^1, \mathbb{A}^1, \mathbb{B}^1)$, and $(\mathbb{D}^2, \mathbb{A}^2, \mathbb{B}^2)$ obtained from the resolution of $\left(\mathcal{P}^{1^{st}}_{order}\right)$, $\left(\mathcal{P}^{2^{nd}}_{order}\right)$, and $\left(\mathcal{P}^{3^{rd}}_{order}\right)$, respectively.

The proposed estimates in the composite read:

$$\left.\begin{aligned}\boldsymbol{u}^{est}(\boldsymbol{x},\boldsymbol{y}) &= \boldsymbol{U}(\boldsymbol{x}) \\ &+ \epsilon\, \mathbb{D}^0(\boldsymbol{y}) : \boldsymbol{E}(\boldsymbol{x}) \\ &+ \epsilon^2\, \mathbb{D}^1(\boldsymbol{y}) \vdots \boldsymbol{\nabla}_{\boldsymbol{x}}\boldsymbol{E}(\boldsymbol{x}) \\ &+ \epsilon^3\, \mathbb{D}^2(\boldsymbol{y}) :: \boldsymbol{\nabla}_{\boldsymbol{x}}\boldsymbol{\nabla}_{\boldsymbol{x}}\boldsymbol{E}(\boldsymbol{x})\end{aligned}\right\} \quad \forall \boldsymbol{x} \in \Omega,\ \forall \boldsymbol{y} \in Y, \tag{22}$$

$$\left.\begin{aligned}\boldsymbol{\varepsilon}^{est}(\boldsymbol{x},\boldsymbol{y}) &= \mathbb{A}^0(\boldsymbol{y}) : \boldsymbol{E}(\boldsymbol{x}) \\ &+ \epsilon\, \mathbb{A}^1(\boldsymbol{y}) \vdots \boldsymbol{\nabla}_{\boldsymbol{x}}\boldsymbol{E}(\boldsymbol{x}) \\ &+ \epsilon^2\, \mathbb{A}^2(\boldsymbol{y}) :: \boldsymbol{\nabla}_{\boldsymbol{x}}\boldsymbol{\nabla}_{\boldsymbol{x}}\boldsymbol{E}(\boldsymbol{x})\end{aligned}\right\} \quad \forall \boldsymbol{x} \in \Omega,\ \forall \boldsymbol{y} \in Y, \tag{23}$$

$$\left.\begin{aligned}\boldsymbol{\sigma}^{est}(\boldsymbol{x},\boldsymbol{y}) &= \mathbb{B}^0(\boldsymbol{y}) : \boldsymbol{E}(\boldsymbol{x}) \\ &+ \epsilon\, \mathbb{B}^1(\boldsymbol{y}) \vdots \boldsymbol{\nabla}_{\boldsymbol{x}}\boldsymbol{E}(\boldsymbol{x}) \\ &+ \epsilon^2\, \mathbb{B}^2(\boldsymbol{y}) :: \boldsymbol{\nabla}_{\boldsymbol{x}}\boldsymbol{\nabla}_{\boldsymbol{x}}\boldsymbol{E}(\boldsymbol{x})\end{aligned}\right\} \quad \forall \boldsymbol{x} \in \Omega,\ \forall \boldsymbol{y} \in Y. \tag{24}$$

3. Boundary layer correction

While asymptotic homogenization may provide an accurate estimate of local fields within the structure based on a relocalization process, the construction of a solution near the boundaries remains beyond its capability. This is mainly explained by the loss of the periodicity assumption in the vicinity of boundaries.

Fergoug et al. (2022) have proposed a new approach to correct first-order estimates, constructed by a first-order relocalization process. This approach is based on the idea of introducing corrective terms that would decay inward the material, far from boundaries. These terms are obtained from the resolution of various problems over

the unit-cell. The nature of the problems to be solved depends on the actual boundary conditions applied to the structure. The proposed approach is general, *i.e.* valid for different BCs: Dirichlet, Neumann or mixed.

In this section, an extension of this method is proposed to correct higher-order estimated fields, $(\boldsymbol{u}^{est}, \boldsymbol{\varepsilon}^{est}, \boldsymbol{\sigma}^{est})$ defined in Eq. (22), (23), (24), respectively. To do so, supplementary problems over the unit-cell, beside those of a first-order correction, must be considered: 18 additional problems for a second-order correction and 54 for a third-order correction.

3.1. Correctors for Neumann BCs

The homogenized problem $(\mathcal{P}_{hom})$ can be written as:

$$\begin{cases} \operatorname{div}\left(\boldsymbol{\Sigma}\left(\boldsymbol{x}\right)\right) + \boldsymbol{f}\left(\boldsymbol{x}\right) = 0, & \forall \boldsymbol{x} \in \boldsymbol{\Omega}, \quad (25a) \\ \boldsymbol{\Sigma}\left(\boldsymbol{x}\right) = \mathbb{C}^0 : \boldsymbol{E}\left(\boldsymbol{x}\right), & \forall \boldsymbol{x} \in \boldsymbol{\Omega}, \quad (25b) \\ \boldsymbol{U}\left(\boldsymbol{x}\right) = \boldsymbol{u}^d, & \forall \boldsymbol{x} \in \boldsymbol{\Gamma}_{\boldsymbol{u}}, \quad (25c) \\ \boldsymbol{\Sigma}\left(\boldsymbol{x}\right) \cdot \boldsymbol{n} = \boldsymbol{F}^d, & \forall \boldsymbol{x} \in \boldsymbol{\Gamma}_{\boldsymbol{t}}, \quad (25d) \end{cases}$$

with the macroscale stress: $\langle \boldsymbol{\sigma}^{est} \rangle_Y = \boldsymbol{\Sigma}$ and strain: $\langle \boldsymbol{\varepsilon}^{est} \rangle_Y = \boldsymbol{E}$.

It is apparent from problem (25d) that the boundary condition on $\boldsymbol{\Gamma}_{\boldsymbol{t}}$ is only satisfied by the mean value of $\boldsymbol{\sigma}^{est}$, therefore, in general:

$$\boldsymbol{\sigma}^{est} \cdot \boldsymbol{n} \neq \boldsymbol{F}^d. \quad (26)$$

Corrective term $\boldsymbol{\sigma}^{bl}$ is introduced, whose sum with the estimated stress field $\boldsymbol{\sigma}^{est}$ satisfies exactly the Neumann boundary condition at each microscopic point, then:

$$\left(\boldsymbol{\sigma}^{est} + \boldsymbol{\sigma}^{bl}\right) \cdot \boldsymbol{n} = \boldsymbol{F}^d. \quad (27)$$

We propose to compute $\boldsymbol{\sigma}^{bl}$ by considering auxiliary problems on the unit-cell, subjected to characteristic loads F_i with $i \in \{1,2,3\}$ where the Neumann boundary condition is applied. The opposite surface is fixed, and other remaining surfaces are subjected to periodicity conditions (see (Fergoug et al., 2022) for more details). The expression of characteristic loads depends on the order of the boundary correction:

- First-order corrective load:

$$F^0_{ikl} = -B^0_{ijkl} \cdot n_j + \frac{1}{|Y|} \int_Y B^0_{ijkl} \cdot n_j \, dY, \text{ with fixed index } j. \tag{28}$$

B^0_{ijkl} are components of the first-order stress localization tensor $\mathbb{B}^0$ and $kl = \{11, 22, 33, 23, 31, 12\}_6$. Therefore, 6 loads are applied successively over the unit-cell.

- Second-order corrective load:

$$F^1_{iklm} = -B^1_{ijklm} \cdot n_j + \frac{1}{|Y|} \int_Y B^1_{ijklm} \cdot n_j \, dY, \text{ with fixed index } j. \tag{29}$$

B^1_{ijklm} are components of the second-order stress localization tensor $\mathbb{B}^1$ and $klm = \{111, 211, 311, ..., 112, 212, 312\}_{18}$. Therefore, 18 loads are applied successively over the unit-cell.

- Third-order corrective load:

$$F^2_{iklmn} = -B^2_{ijklmn} \cdot n_j + \frac{1}{|Y|} \int_Y B^2_{ijklmn} \cdot n_j \, dY, \text{ with fixed index } j. \tag{30}$$

B^2_{ijklmn} are components of the third-order stress localization tensor $\mathbb{B}^2$ and $klmn = \{1111, 2111, 3111, ..., 1312, 2312, 3312\}_{54}$. Therefore, 54 loads are applied successively over the unit-cell.

Note that n_j is the normal direction of $\mathbf{\Gamma_t}$ and the fixed index $j \in \{1, 2, 3\}$ is the index of this normal direction.

The resulting displacement, strain, and stress fields obtained for each loading case provide a component of first, second, or third order boundary layer displacement, strain, and stress localization tensors $(\mathbb{D}^{0,bl}, \mathbb{A}^{0,bl}, \mathbb{B}^{0,bl})$, $(\mathbb{D}^{1,bl}, \mathbb{A}^{1,bl}, \mathbb{B}^{1,bl})$, and $(\mathbb{D}^{2,bl}, \mathbb{A}^{2,bl}, \mathbb{B}^{2,bl})$, respectively.

Therefore, the boundary layer correctors read:

$$\left.\begin{aligned} \boldsymbol{u}^{bl}(\boldsymbol{x},\boldsymbol{y}) &= \epsilon \mathbb{D}^{0,bl}(\boldsymbol{y}) : \boldsymbol{E}(\boldsymbol{x}) \\ &+ \epsilon^2\, \mathbb{D}^{1,bl}(\boldsymbol{y}) \vdots \boldsymbol{\nabla}_{\boldsymbol{x}} \boldsymbol{E}(\boldsymbol{x}) \\ &+ \epsilon^3\, \mathbb{D}^{2,bl}(\boldsymbol{y}) :: \boldsymbol{\nabla}_{\boldsymbol{x}} \boldsymbol{\nabla}_{\boldsymbol{x}} \boldsymbol{E}(\boldsymbol{x}) \end{aligned}\right\} \quad \forall \boldsymbol{x} \in \mathbf{\Gamma_t},\ \forall \boldsymbol{y} \in Y, \tag{31}$$

$$\left.\begin{aligned} \boldsymbol{\varepsilon}^{bl}(\boldsymbol{x},\boldsymbol{y}) &= \mathbb{A}^{0,bl}(\boldsymbol{y}) : \boldsymbol{E}(\boldsymbol{x}) \\ &+ \epsilon\, \mathbb{A}^{1,bl}(\boldsymbol{y}) \vdots \boldsymbol{\nabla}_{\boldsymbol{x}} \boldsymbol{E}(\boldsymbol{x}) \\ &+ \epsilon^2\, \mathbb{A}^{2,bl}(\boldsymbol{y}) :: \boldsymbol{\nabla}_{\boldsymbol{x}} \boldsymbol{\nabla}_{\boldsymbol{x}} \boldsymbol{E}(\boldsymbol{x}) \end{aligned}\right\} \quad \forall \boldsymbol{x} \in \mathbf{\Gamma_t},\ \forall \boldsymbol{y} \in Y, \tag{32}$$

$$\left.\begin{aligned} \boldsymbol{\sigma}^{bl}(\boldsymbol{x},\boldsymbol{y}) &= \mathbb{B}^{0,bl}(\boldsymbol{y}) : \boldsymbol{E}(\boldsymbol{x}) \\ &+ \epsilon\, \mathbb{B}^{1,bl}(\boldsymbol{y}) \vdots \boldsymbol{\nabla}_{\boldsymbol{x}} \boldsymbol{E}(\boldsymbol{x}) \\ &+ \epsilon^2\, \mathbb{B}^{2,bl}(\boldsymbol{y}) :: \boldsymbol{\nabla}_{\boldsymbol{x}} \boldsymbol{\nabla}_{\boldsymbol{x}} \boldsymbol{E}(\boldsymbol{x}) \end{aligned}\right\} \quad \forall \boldsymbol{x} \in \mathbf{\Gamma_t},\ \forall \boldsymbol{y} \in Y. \tag{33}$$

As a result, the stress field $\boldsymbol{\sigma}^{cor}$

$$\boldsymbol{\sigma}^{cor} = \boldsymbol{\sigma}^{est} + \boldsymbol{\sigma}^{bl}, \tag{34}$$

satisfies the Neumann BC.

Remark 1. *In order to manage boundaries which are neither vertical nor horizontal, one can write the following tensors:*

$$\begin{cases} \mathbb{F}^0 = -\mathbb{B}^0 \cdot \boldsymbol{n} + \dfrac{1}{|Y|}\displaystyle\int_Y \mathbb{B}^0 \cdot \boldsymbol{n}\ dY, & \text{(35a)} \\ \mathbb{F}^1 = -\mathbb{B}^1 \cdot \boldsymbol{n} + \dfrac{1}{|Y|}\displaystyle\int_Y \mathbb{B}^1 \cdot \boldsymbol{n}\ dY, & \text{(35b)} \\ \mathbb{F}^2 = -\mathbb{B}^2 \cdot \boldsymbol{n} + \dfrac{1}{|Y|}\displaystyle\int_Y \mathbb{B}^2 \cdot \boldsymbol{n}\ dY, & \text{(35c)} \end{cases}$$

where $\mathbb{F}^0$, $\mathbb{F}^1$ and $\mathbb{F}^2$ are third, fourth and fifth-rank tensors, respectively. Corrective loads to be applied over the unit-cell, for different orders, are the components of these tensors. For instance, the normal vector $\boldsymbol{n}$ will be equal to $\frac{1}{\sqrt{2}}\begin{pmatrix}1 & 1 & 0\end{pmatrix}^\top$ in the case of a macroscopic boundary that has a $45°$ boundary.

3.2. Correctors for Dirichlet BCs

It is clear from (25c) that the homogenized displacement field $\boldsymbol{U}$ verifies the Dirichlet BC, *i.e.* $\boldsymbol{U} = \boldsymbol{u}^d$ on $\boldsymbol{\Gamma}_{\boldsymbol{u}}$. Therefore, $\boldsymbol{u}^{est}$ defined in Eq. (22) does not necessarily satisfy this BC. Therefore, a correction is needed that verifies:

$$\boldsymbol{u}^{cor}(\boldsymbol{x},\boldsymbol{y}) = \boldsymbol{U}(\boldsymbol{x}) + \Big(\boldsymbol{v}(\boldsymbol{x},\boldsymbol{y}) + \boldsymbol{u}^{bl}(\boldsymbol{x},\boldsymbol{y})\Big), \tag{36}$$

where the periodic fluctuation $\boldsymbol{v}$ reads:

$$\boldsymbol{v} = \ \epsilon\boldsymbol{u}^1(\boldsymbol{x},\boldsymbol{y}) + \epsilon^2\boldsymbol{u}^2(\boldsymbol{x},\boldsymbol{y}) + \epsilon^3\boldsymbol{u}^3(\boldsymbol{x},\boldsymbol{y}), \tag{37}$$

then

$$\begin{aligned} \boldsymbol{v} =& \epsilon\ \mathbb{D}^0(\boldsymbol{y}) : \boldsymbol{E}(\boldsymbol{x}) \\ &+ \epsilon^2\ \mathbb{D}^1(\boldsymbol{y}) \vdots \boldsymbol{\nabla}_{\boldsymbol{x}}\boldsymbol{E}(\boldsymbol{x}) \\ &+ \epsilon^3\ \mathbb{D}^2(\boldsymbol{y}) :: \boldsymbol{\nabla}_{\boldsymbol{x}}\boldsymbol{\nabla}_{\boldsymbol{x}}\boldsymbol{E}(\boldsymbol{x}). \end{aligned} \tag{38}$$

The correction $\boldsymbol{u}^{bl}$ must verify:

$$\boldsymbol{u}^{bl}\left(\boldsymbol{x},\boldsymbol{y}\right)=-\boldsymbol{v}\left(\boldsymbol{x},\boldsymbol{y}\right),\qquad\forall\boldsymbol{x}\in\boldsymbol{\Gamma}_{\boldsymbol{u}},\ \forall\boldsymbol{y}\in Y. \tag{39}$$

Similarly to the Neumann boundary case, several auxiliary problems are considered providing boundary layer correctors. In this case, corrective displacements ϱ_i with $i\in\{1,2,3\}$ are applied to the unit-cell and defined as:

- First-order corrective displacement:

$$\varrho^0_{ikl}=-D^0_{ikl}, \tag{40}$$

with $kl=\{11,22,33,23,31,12\}_6$ and D^0_{ikl} are components of the first-order displacement localization tensor $\mathbb{D}^0$.

- Second-order corrective displacement:

$$\varrho^1_{iklm}=-D^1_{iklm}, \tag{41}$$

with $klm=\{111,211,311,...,112,212,312\}_{18}$ and D^1_{iklm} are components of the second-order displacement localization tensor $\mathbb{D}^1$.

- Third-order corrective displacement:

$$\varrho^2_{iklmn}=-D^2_{iklmn}, \tag{42}$$

with $klmn=\{1111,2111,3111,...,1312,2312,3312\}_{54}$ and D^2_{iklmn} are components of the third-order displacement localization tensor $\mathbb{D}^2$.

The corrective boundary layer fields are obtained by conducting the same analyses defined in Eq. (31), (32), and (33).

Remark 2. *We recall that in order to compute boundary layer localization tensors, for a Neumann boundary conditions, at different orders:* $(\mathbb{D}^{0,bl}, \mathbb{A}^{0,bl}, \mathbb{B}^{0,bl})$, $(\mathbb{D}^{1,bl}, \mathbb{A}^{1,bl}, \mathbb{B}^{1,bl})$, *and* $(\mathbb{D}^{2,bl}, \mathbb{A}^{2,bl}, \mathbb{B}^{2,bl})$, *auxiliary problems, over the unit-cell, are considered where the applied loads* F^0_{ikl}, F^1_{iklm} *and* F^2_{iklmn} *are defined in Eq. (28), (29), and (30), respectively. Similarly for Dirichlet boundary conditions, displacement fields* ϱ^0_{ikl}, ϱ^1_{iklm}, *and* ϱ^2_{iklmn}, *defined in Eq. (40), (41), and (42), are applied on the unit-cell. Details concerning the formulation of auxiliary problems, at the first-order, are provided in Fergoug et al. (2022), and are omitted here for higher-orders for the sake of conciseness.*

Remark 3. *For mixed BCs, the correction is derived by applying both characteristic load* F_i *and displacement* ϱ_i. *The correction to be ultimately applied depends on the actual (Neumann or Dirichlet) BC applied in this specific direction. For more details, the reader is referred to Fergoug et al. (2022).*

4. Numerical implementation

The objective of the relocalization process is to compute estimated fields $(\boldsymbol{u}^{est}, \boldsymbol{\varepsilon}^{est}, \boldsymbol{\sigma}^{est})$ defined in Eq. (22), (23), (24), respectively. To do so, three hierarchical sets of elasticity problems are solved over the unit-cell, with applied Periodic Boundary Conditions (PBC):

- **First-order problem** $\left(\mathcal{P}^{1^{st}}_{order}\right)$: After discretizing the unit-cell domain, six linearly independent unit strain loads are applied (for 3D cases). By using the modified Voigt notations, the macroscale strain field reads:

$$\boldsymbol{E} = \left(E_{11}, E_{22}, E_{33}, \sqrt{2}E_{23}, \sqrt{2}E_{31}, \sqrt{2}E_{12}\right)_6 . \tag{43}$$

The solutions to these problems are first-order displacement, strain, and stress localization tensors: $\mathbb{D}^0$, $\mathbb{A}^0$, and $\mathbb{B}^0$, respectively. The homogenized elasticity tensor reads: $\mathbb{C}^0 = \langle \mathbb{B}^0(\boldsymbol{y}) \rangle_Y$.

- **Second-order problem** $\left(\mathcal{P}^{2^{nd}}_{order}\right)$: A body force $\boldsymbol{L}^1$ and eigenstrain $\boldsymbol{\eta}^1$ defined in Eq. (9), which depend on the resolution of $\left(\mathcal{P}^{1^{st}}_{order}\right)$, are prescribed over the unit-cell. Since these enforcing terms are connected with the gradient of strain $\boldsymbol{E}$, then one should apply 18 loads on the unit-cell. Indeed, $\boldsymbol{\nabla}_x \boldsymbol{E}$ is symmetric according to its first two indices ($E_{ij,k} = E_{ji,k}$), then it is possible to represent it by a vector of dimension 18 as:

$$\boldsymbol{\nabla}_x \boldsymbol{E} = \left(E_{11,k}, E_{22,k}, E_{33,k}, \sqrt{2}E_{23,k}, \sqrt{2}E_{31,k}, \sqrt{2}E_{12,k}\right)_{18}, \text{ with } k = 1,2,3. \quad (44)$$

The solutions to these problems are second-order displacement, strain, and stress localization tensors: $\mathbb{D}^1$, $\mathbb{A}^1$, and $\mathbb{B}^1$, respectively.

- **Third-order problem** $\left(\mathcal{P}^{3^{rd}}_{order}\right)$: A body force $\boldsymbol{L}^2$ and eigenstrain $\boldsymbol{\eta}^2$ defined in Eq. (16), which depend on the resolution of $\left(\mathcal{P}^{2^{nd}}_{order}\right)$, are prescribed over the unit-cell. Since these enforcing terms are connected with the second gradient of strain $\boldsymbol{E}$, one should apply 54 loads on the unit-cell. Indeed, $\boldsymbol{\nabla}_x \boldsymbol{\nabla}_x \boldsymbol{E}$ can be represented by a vector of dimension 54:

$$\boldsymbol{\nabla}_x \boldsymbol{\nabla}_x \boldsymbol{E} = \left(E_{11,kj}, E_{22,kj}, E_{33,kj}, \sqrt{2}E_{23,kj}, \sqrt{2}E_{31,kj}, \sqrt{2}E_{12,kj}\right)_{54}, \text{ with } k,j = 1,2,3. \quad (45)$$

The solutions to these problems are third-order displacement, strain, and stress localization tensors: $\mathbb{D}^2$, $\mathbb{A}^2$, and $\mathbb{B}^2$, respectively.

Remark 4. *From a practical standpoint, solving* $\left(\mathcal{P}^{1^{st}}_{order}\right)$, $\left(\mathcal{P}^{2^{nd}}_{order}\right)$ *and* $\left(\mathcal{P}^{3^{rd}}_{order}\right)$ *corresponds to subjecting the unit-cell to 6, 18 or 54 gradients of various order of the strain field.*

Remark 5. *Localization tensors, of various orders, are functions of microstructural characteristics only, and independent of the homogenized problem. Thus, these quantities are computed only once for each type of unit-cell.*

After discretizing the macroscale mesh, one can solve the homogenized problem ($\mathcal{P}_{hom}$) whose solution fields are $(\boldsymbol{U}, \boldsymbol{E}, \boldsymbol{\Sigma})$. Successive macroscale strain gradients are used to compute estimated fields defined in Eq. (22), (23), (24).

Remark 6. *Successive gradients of macroscale strain, involved in higher-order relocalization processes, are resolved numerically. For instance, the gradient of macroscale strain field, $\nabla_x \boldsymbol{E}$, has been evaluated by extrapolating corresponding strain values between integration points to the nodes and then appropriately differentiating them using the usual finite element shape functions. The same procedure is used to evaluate the second gradient of macroscale strain field $\nabla_x \nabla_x \boldsymbol{E}$. Sufficient order of finite element shape functions are required.*

To eliminate mesh sensitivity and facilitate the computation of error estimates, we consider that the macroscale mesh is identical to the microscale one, but endowed with homogenized properties. If not, a mapping of the homogeneous fields on the microscale mesh could be considered as shown by Kruch (2007). An intermediate step is then considered to locate each unit-cell on the macroscale mesh as in Fergoug et al. (2022).

The relocalization process improvement proposed by Kruch and Forest (1998) is considered. Estimated fields, in a given point of the unit-cell, are determined using localization tensors combined with the value of the current macroscale strain or its gradients *at this point*, and not its average over the unit-cell.

Once homogenization problems are solved, localization tensors are used to construct corrective loads and displacements for the boundary layer correction. After-

wards, boundary layer localization tensors $(\mathbb{D}^{0,bl}, \mathbb{A}^{0,bl}, \mathbb{B}^{0,bl})$, $(\mathbb{D}^{1,bl}, \mathbb{A}^{1,bl}, \mathbb{B}^{1,bl})$ and $(\mathbb{D}^{2,bl}, \mathbb{A}^{2,bl}, \mathbb{B}^{2,bl})$ are computed and used to compute boundary layer correctors defined in Eq. (31), (32), and (33).
Higher-order relocalization and boundary layer correction processes are summarized in Fig. 2.

5. Numerical examples

To demonstrate the effectiveness of the proposed relocalization and boundary layer correction processes, two numerical examples of composite structures in linear elasticity are presented.
In these examples, we will compare the following fields:

- Microscale fields obtained by solving problem $(\mathcal{P}_{ref})$ using DNS, which will be considered as our reference, indexed *ref*.
- Homogeneous fields obtained by solving problem $(\mathcal{P}_{hom})$, indexed *hom*.
- Proposed first, second, and third-order estimates of microscale fields obtained by the first, second, and third-order relocalization processes, indexed *est1*, *est2*, and *est3*, respectively.
- Proposed first, second, and third-order boundary layer corrections of estimated fields indexed *cor1*, *cor2*, and *cor3*, respectively.

We will also quantify the difference between the reference and estimated fields by computing the modeling error. For this purpose, the following local (element-wise)

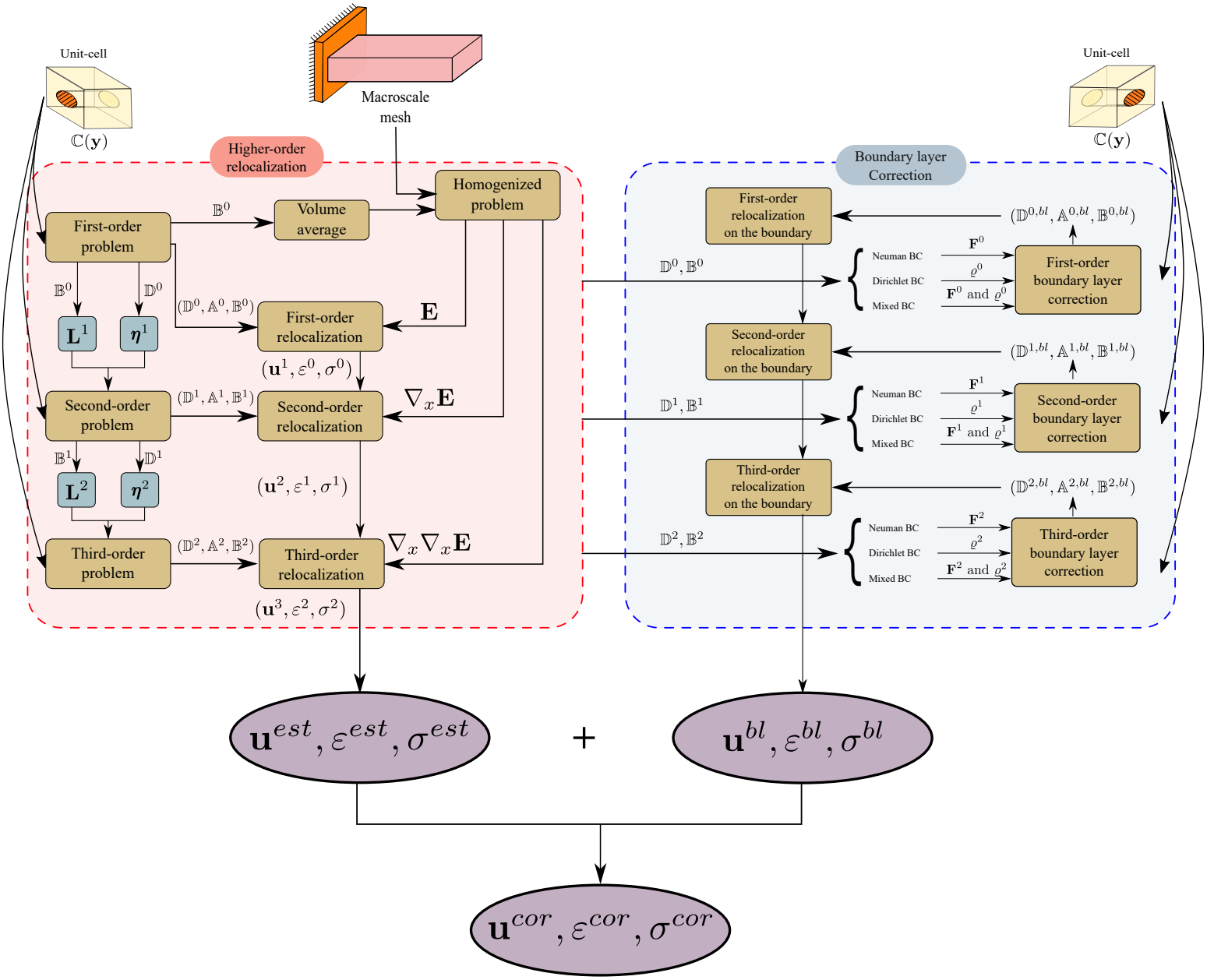

Figure 2: Workflow describing higher-order relocalization and boundary layer correction processes.

error in energy norm is defined:

$$\begin{aligned} \|\boldsymbol{e}\|_{E(\Omega_e)} &= \|\boldsymbol{u}^{ref}(\boldsymbol{x}) - \boldsymbol{u}^{k}(\boldsymbol{x})\|_{E(\Omega_e)} \\ &= \left(\int_{\Omega_e} \nabla^s \left(\boldsymbol{u}^{ref}(\boldsymbol{x}) - \boldsymbol{u}^{k}(\boldsymbol{x})\right) \vdots \mathbb{C} : \nabla^s \left(\boldsymbol{u}^{ref}(\boldsymbol{x}) - \boldsymbol{u}^{k}(\boldsymbol{x})\right) d\Omega_e\right)^{\frac{1}{2}}, \end{aligned} \tag{46}$$

where Ω_e denotes the domain of an element and $\boldsymbol{u}^k(\boldsymbol{x})$ denotes the estimated displacement field whose error is measured. The global error $\|\boldsymbol{e}\|_{E(\Omega)}$ is then defined as:

$$\|\boldsymbol{e}\|^2_{E(\Omega)} = \sum_e \|\boldsymbol{e}\|^2_{E(\Omega_e)}. \tag{47}$$

5.1. Laminated composite in bending

We consider a plane strain elasticity problem of a laminated composite made of two layers as presented in Fig. 3. The size of the structure is $L = 8$ mm, $H = 5$ mm and $W = 1$ mm. The two layers are assumed to be isotropic linear elastic with coefficients $(E_m = 500 \text{ MPa}, \nu_m = 0.3)$ and $(E_f = 5000, \nu_f = 0.3)$.

In this example, we consider that $\epsilon = 1$. Therefore, mechanical fields depend only

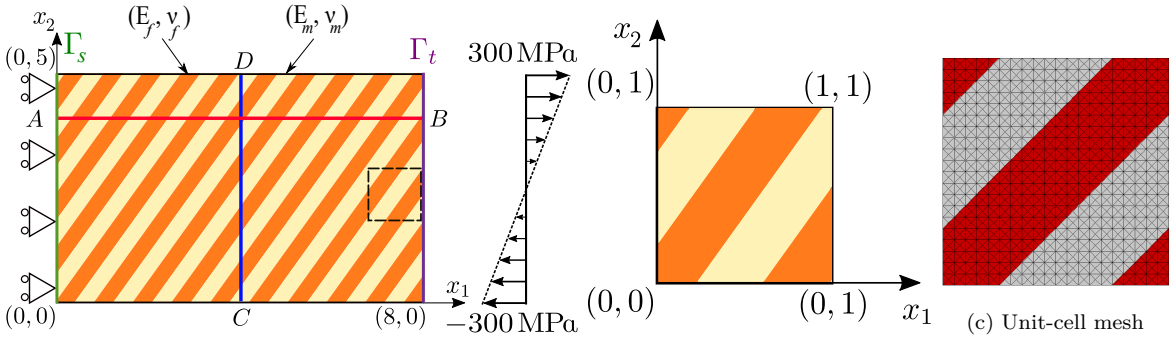

(a) Structure geometry

(b) Unit-cell domain

(c) Unit-cell mesh

Figure 3: Illustration of the laminated composite subjected to bending. The structure is sliding on Γ_s and a surface bending is applied on Γ_t. Other boundaries are kept free of forces. Results will be plotted along AB and CD lines. Boundary layer correctors will be plotted for the boundary cell with dashed line.

on $\boldsymbol{x}$, representing *both* microscale and macroscale coordinates. The finite element mesh describing the unit-cell is composed of 1600 fifteen-node wedge element as shown in Fig. 3. Therefore the mesh describing the entire structure including all

heterogeneities is composed of 64 000 elements, corresponding to 867 909 degrees of freedom.

Remark 7. *In order to correct the mixed boundary Γ_s, it is necessary to apply both the Neumann and Dirichlet boundary corrections.*

5.1.1. Comparison of stress fields

Comparison of resulting stress fields along AB and CD lines are presented in Fig. 4. First-order estimates, *i.e.* σ_{11}^{est1} and σ_{12}^{est1}, obtained by the first-order relocalization process, are inaccurate in the inner domain of the structure. This is mainly explained by high macroscale strain gradients induced by the bending and neglected by a classical first-order relocalization.

We propose to conduct a higher-order relocalization process, up to the third-order, to introduce the effects of macroscale strain gradients. As noticed in Fig. 6, second-order estimates, *i.e.* σ_{11}^{est2} and σ_{12}^{est2}, and third-order estimates, *i.e.* σ_{11}^{est3} and σ_{12}^{est3}, perfectly coincide with the reference inside the structure.

Remark 8. *In this example, the contribution of a third-order relocalization is negligible compared to a second-order relocalization. This is explained by the low second gradient of macroscale strain field, $\nabla_x \nabla_x \boldsymbol{E}$, induced by the bending. For the sake of conciseness, upcoming analyses will be restricted up to the second-order.*

The estimated fields lose their accuracy near the boundaries. This is due to the loss of periodicity in the vicinity of these regions.

We propose a boundary layer correction method based on the computation of corrective terms, that decay toward the interior of the body. Figures 5a and 5b show first and second-order boundary layer correctors σ_{11}^{bl1}, and σ_{11}^{bl2}, respectively. The decay of both boundary corrections takes place over one unit-cell. These corrective terms are

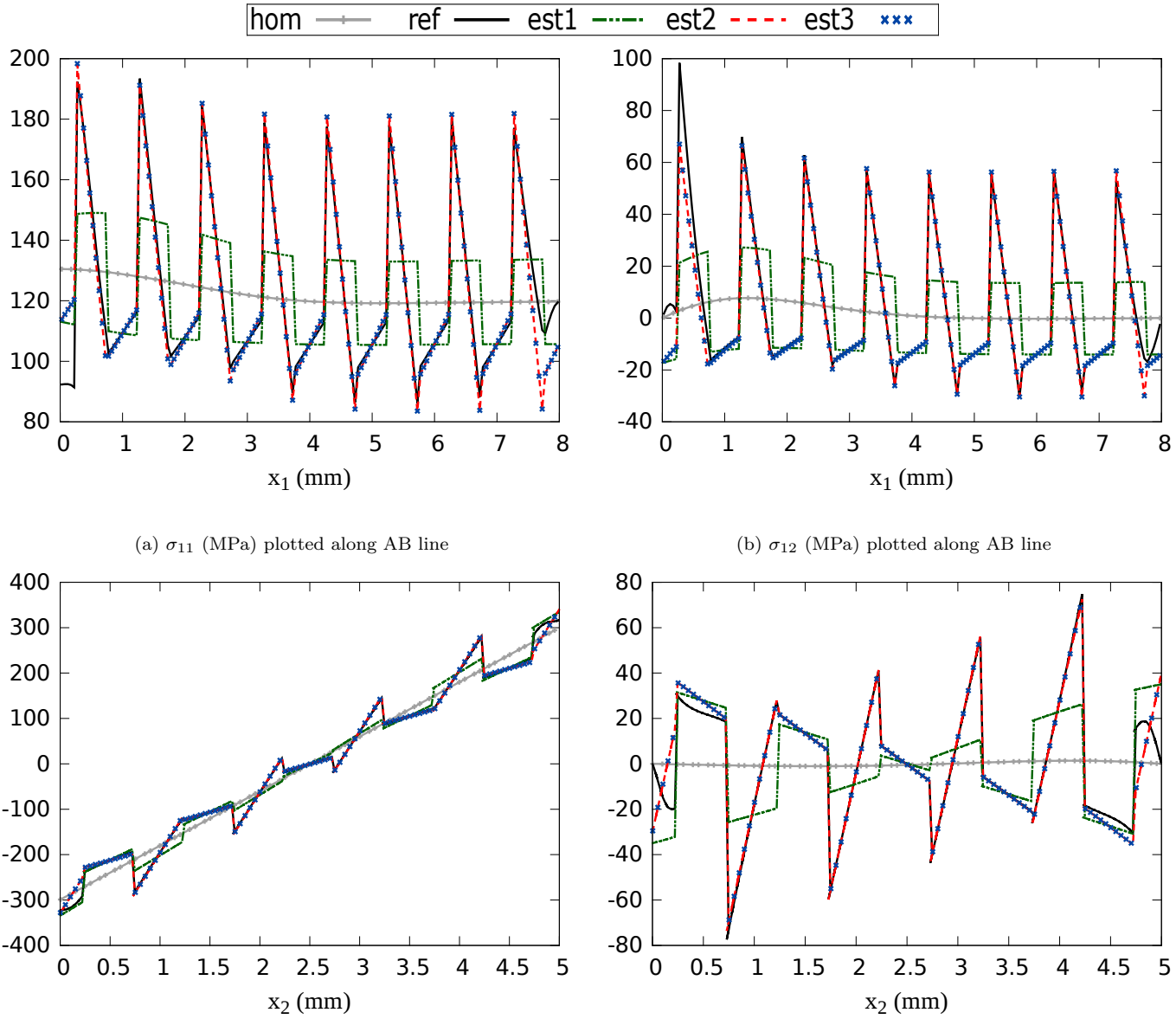

(a) σ_{11} (MPa) plotted along AB line

(b) σ_{12} (MPa) plotted along AB line

(c) σ_{11} (MPa) plotted along CD line

(d) σ_{12} (MPa) plotted along CD line

Figure 4: Results of the homogenized (hom) and reference (ref) fields compared with the first-order ($est1$), second-order ($est2$), and third-order ($est3$) estimates for the laminated composite in bending.

added to the estimated fields obtained from the relocalization processes.

First-order ($cor1$) and second-order ($cor2$) corrected fields plotted along AB and

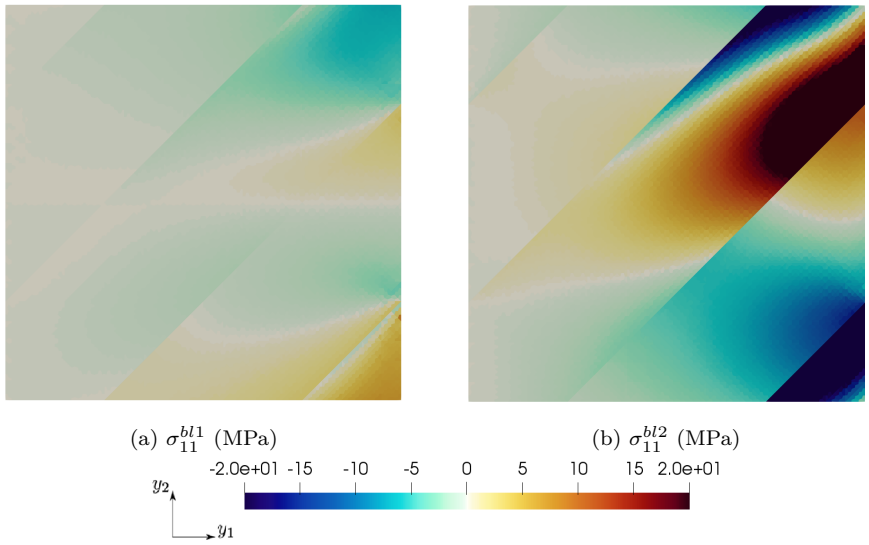

Figure 5: First-order (σ_{11}^{bl1}) and second-order (σ_{11}^{bl2}) boundary layer correctors for the boundary cell with dashed line in Fig. 3. The decay inward (left side of the unit-cell) of both boundary corrections takes place over one unit-cell.

CD lines are presented in Fig. 6.

Remark 9. *Boundary layer correctors are introduced at each order. Thus, for instance:* $\sigma_{11}^{cor1} = \sigma_{11}^{est1} + \sigma_{11}^{bl1}$, *and* $\sigma_{11}^{cor2} = \sigma_{11}^{cor1} + \sigma_{11}^{bl2}$.

First-order corrected fields are still inaccurate on the boundaries, contrarily to second-order corrected fields which are in a good agreement with the reference fields. In particular, σ_{11}^{cor2} verifies the applied Neumann condition at $x_1 = 8$ mm similarly to the reference and the homogeneous counterparts, but it is not the case for σ_{11}^{est1}. We also notice that high stresses are developed inside the structure *and* in the vicinity of the sliding boundary Γ_s as shown in figure 6, which may result in underestimating failure criteria if the design is conducted without the higher-order relocalization and

boundary layer correction.

More precise quantification of the error is provided in the next subsection.

5.1.2. Modeling error

Local relative modeling error between the reference and first-order relocalized fields, before and after the boundary layer correction, are shown in Fig. 7a and 7b, respectively. After the boundary layer correction, the error is reduced on the boundaries, yet still spread inside the structure. For second-order fields, the error before the correction (Fig. 7c), is negligible in the inner domain of the structure, but significant on the boundaries, especially in the vicinity of the sliding boundary Γ_s. After the correction, the modeling error is drastically reduced, but remains concentrated at the corners, as shown in Fig. 7d.

Remark 10. *A particular treatment was considered for corner cells correction, as explained by Fergoug et al. (2022). This correction improves the overall result, yet leaves some residual errors because of the loss of periodicity conditions. Indeed, as shown in Fergoug et al. (2022), Periodic Boundary Conditions (PBC) are not applied for corner cells, contrary to other boundaries where PBC are considered. The corner cells correction can be improved by considering a boundary layer correction applied to two unit-cells instead of one.*

Table 1 summarizes the global relative modeling error for different fields. Second-order relocalization combined with the boundary layer correction allows to drastically reduce the global modeling error by a factor of 3 to 4.

Remark 11. *The use of a Cauchy continuum on the macroscale can lead to errors in the relocalization process for some microstructures and loading conditions as shown in appendix C. In these cases, a higher continuum should considered at the macroscale.*

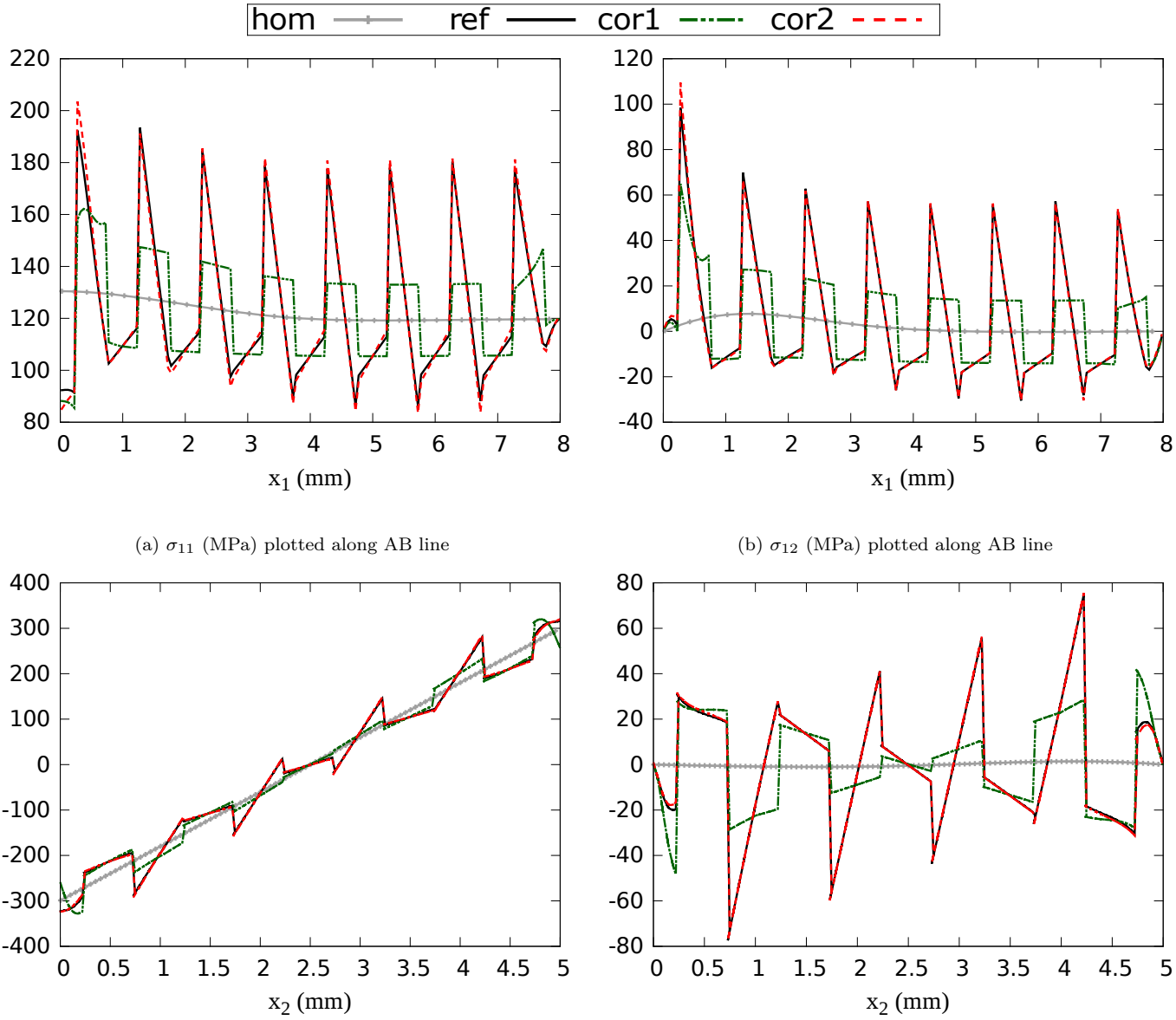

(a) σ_{11} (MPa) plotted along AB line

(b) σ_{12} (MPa) plotted along AB line

(c) σ_{11} (MPa) plotted along CD line

(d) σ_{12} (MPa) plotted along CD line

Figure 6: Results of the homogenized (hom) and reference (ref) fields compared with the corrected first-order ($cor1$), and second-order ($cor2$) estimates for the laminated composite in bending.

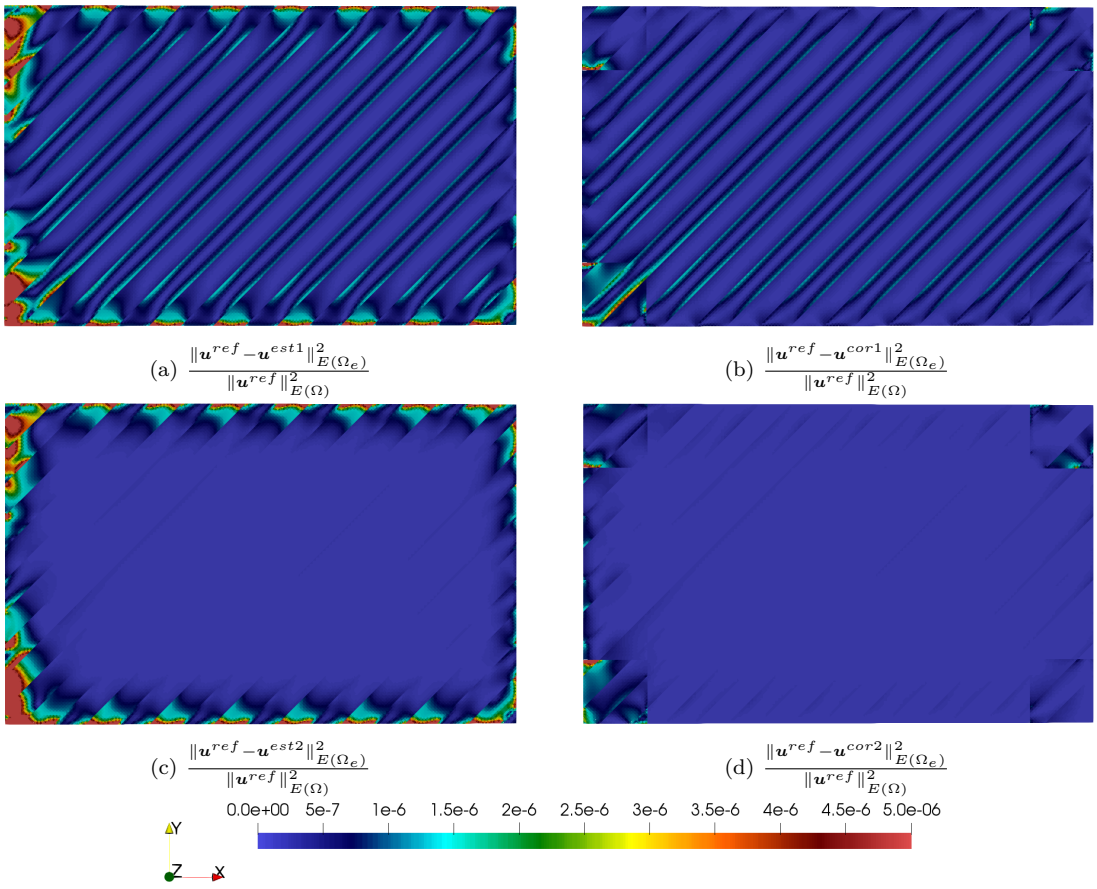

Figure 7: Comparison of the local relative modeling error results for the laminated composite in bending. The modeling error is drastically reduced by increasing the order of the relocalization and boundary layer correction.

Table 1: Comparison of the global relative modeling error for different fields.

Global modeling error	$k = est1$	$k = cor1$	$k = est2$	$k = cor2$
$\frac{\|\boldsymbol{u}^{ref}-\boldsymbol{u}^{k}\|_{E(\Omega)}}{\|\boldsymbol{u}^{ref}\|_{E(\Omega)}}$	16.6%	10.9%	14.4%	4.7%

5.2. Matrix-inclusion composite subjected to prescribed body forces

We consider the in-plane linear elasticity problem of a matrix-inclusion composite, as depicted in Fig. 8, subjected to body forces (f_1 and f_2) in the two space directions, with Γ_u fixed. The size of the structure is $L = 1$ mm and $H = 1$ mm with fiber volume fraction of 0.25; matrix and inclusions are assumed to be isotropic linear elastic with coefficients ($E_m = 1$ MPa, $\nu_m = 1/3$) and ($E_f = 100$, $\nu_f = 1/3$), respectively. In this example, the scale ratio $\epsilon = 1/3$. The finite element mesh describing the unit-cell is composed of 6300 twenty-node brick element element as shown in Fig. 8. Therefore the mesh describing the entire structure including all heterogeneities is composed of 56 700 elements, corresponding to 1 193 409 degrees of freedom.

Body forces are prescribed in the form:

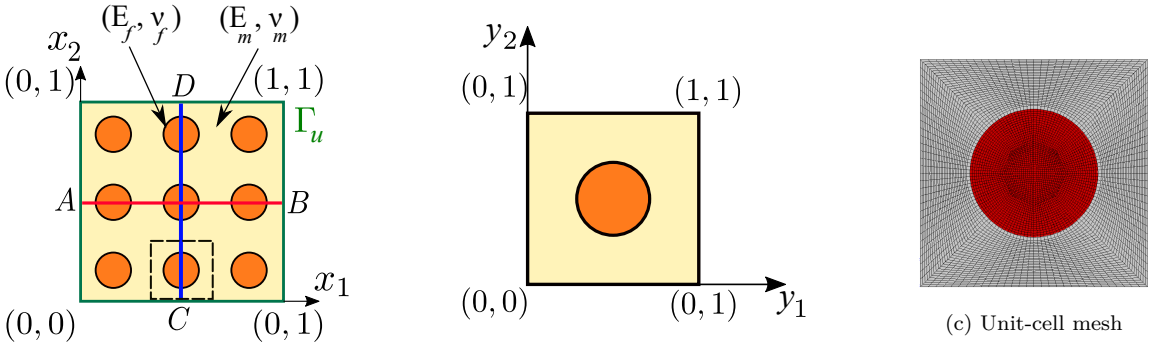

(a) Structure geometry

(b) Unit-cell domain

(c) Unit-cell mesh

Figure 8: Illustration of matrix-inclusion composite. The structure is fixed on Γ_u, body forces f_1 and f_2 are applied in the two directions of space. Results will be plotted along AB and CD lines. Boundary layer correctors will be plotted for the boundary cell with dashed line.

$$\begin{cases} f_1 = \sin(\pi x_1)\sin(\pi x_2) - \dfrac{C^0_{1122} + C^0_{1212}}{C^0_{2222} + C^0_{1212}} \cos(\pi x_1)\cos(\pi x_2), & \text{(48a)} \\ f_2 = \sin(\pi x_1)\sin(\pi x_2) - \dfrac{C^0_{2211} + C^0_{1212}}{C^0_{1111} + C^0_{1212}} \cos(\pi x_1)\cos(\pi x_2). & \text{(48b)} \end{cases}$$

The choice of the applied body forces f_1 and f_2 is justified by the resulting simple analytical solutions obtained for the homogenized problem ($\mathcal{P}_{hom}$). Indeed, the homogenized displacement field is:

$$\begin{cases} U_i = X_i \ \sin(\pi x_1)\sin(\pi x_2), & \text{(49a)} \\ X_1 = \dfrac{1}{\pi^2\left(C^0_{1111}+C^0_{1212}\right)}, \ X_2 = \dfrac{1}{\pi^2\left(C^0_{2222}+C^0_{1212}\right)}, & \text{(49b)} \end{cases}$$

where C^0_{ijkl} are the components of the effective tensor $\mathbb{C}^0$, and the homogenized material is orthotropic.

Remark 12. *Successive gradients of macroscale strain are computed analytically. Therefore, numerical errors resulting from higher-order spatial derivatives of* $\boldsymbol{E}$ *are avoided. In the general case,* $\boldsymbol{E}$ *and its successive gradients must be obtained numerically, as in the previous example 5.1.*

This problem 5.2 has also been treated by He and Pindera (2020b), where a third-order relocalization is performed using a finite volume method. The boundary layer correction is conducted by applying the third-order relocalized displacement field, defined in Eq. 22, in the inner domain of the *fully* detailed, *i.e.* using DNS, boundary. This may be computationally cumbersome when the boundary domain is large. We propose an *alternative* boundary layer method, where corrective terms are obtained by the resolution of independent auxiliary problems over a *single unit-cell*, and then added to the relocalized fields as explained in section 3. The nature of the problems to be solved depends on the actual boundary conditions applied locally to the structure (Fergoug et al., 2022). A comparative study is performed in appendix B.

5.2.1. Comparison of stress fields

Comparisons of stress fields, before the boundary layer correction, along the AB and CD lines are presented in Fig. 9. Second and third-order estimates perfectly co-

incide with reference fields in the inner domain of the composite, but are inaccurate near the boundaries. The first-order estimate, however, provides a poor approximation on the whole plotted domain. It is noticed, in Fig. 9, that third-order estimates provide slightly more accurate solutions than second-order estimates, especially near the boundaries, albeit at a higher computation cost.

First (σ_{11}^{bl1}), second (σ_{11}^{bl2}) and third-order (σ_{11}^{bl3}) boundary layer correctors are shown in figures 10a, 10b, and 10b, respectively. It is observed that the decay of the correction takes place over one unit-cell and becomes less pronounced by increasing the order of the correction.

Comparisons of stress fields, after the boundary layer correction, along the AB and CD lines are presented in Fig. 11. It is showed that corrected fields, near the boundaries, get closer to the reference by increasing the order of the correction.

5.2.2. Modeling error

The local relative modeling error, without the boundary layer correction, is presented in figures 12a, 12b, and 12c. By increasing the order of the relocalization, the error is drastically reduced in the inner domain of the composite, but remains concentrated near the fixed boundary Γ_u.

The local relative modeling error, after the boundary layer correction, is presented in figures 12d, 12e, and 12f. The modeling error significantly decreases near the boundaries, but remains mainly concentrated at the corners.

Table 2 summarizes the global relative modeling error for different fields. The global modeling error is reduced by a factor of 3 to 4 for a third-order relocalization combined with boundary layer correction.

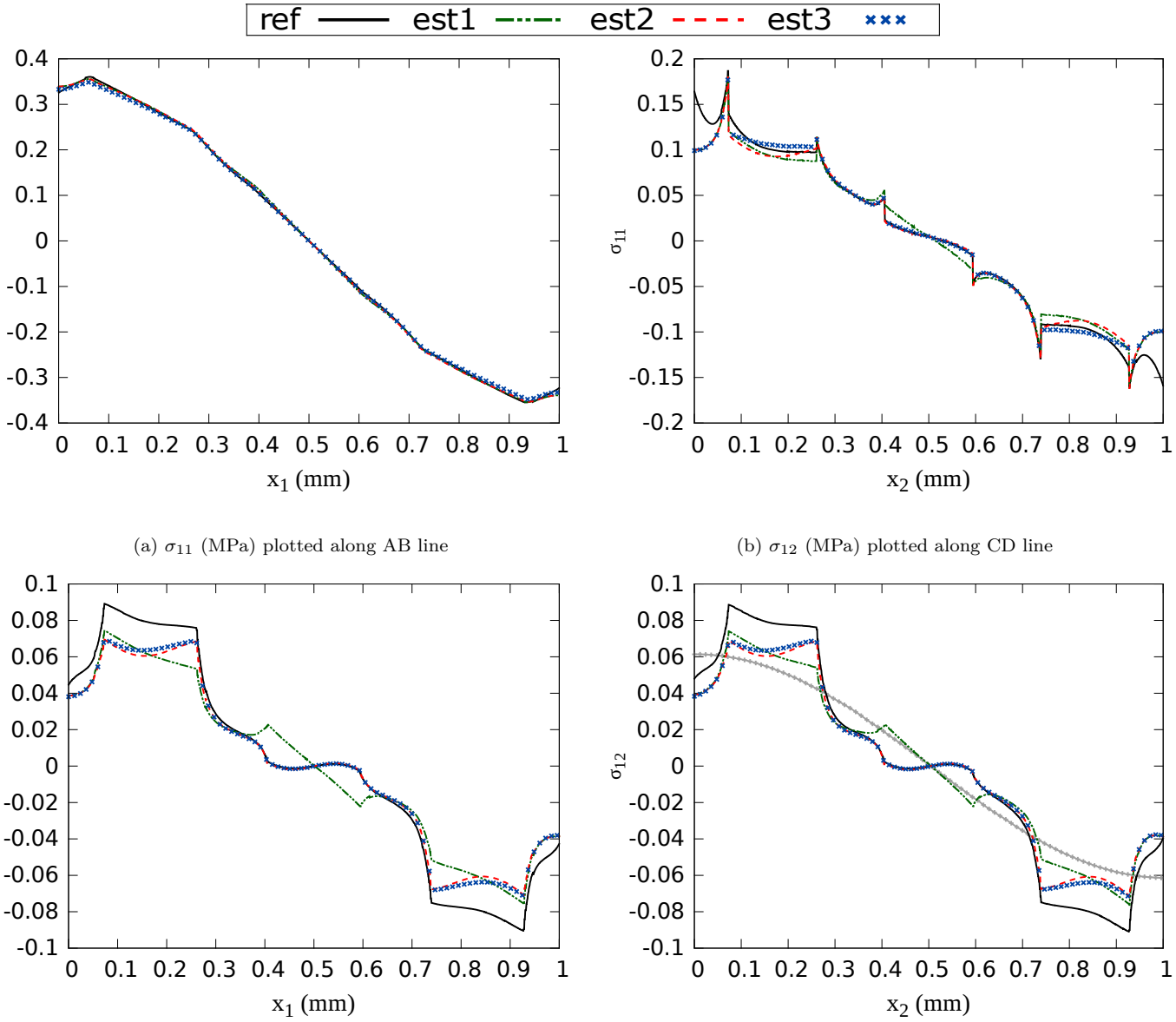

(a) σ_{11} (MPa) plotted along AB line

(b) σ_{12} (MPa) plotted along CD line

(c) σ_{11} (MPa) plotted along AB line

(d) σ_{12} (MPa) plotted along CD line

Figure 9: Results of the reference (ref) field compared with the first-order ($est1$), second-order ($est2$), and third-order ($est3$) estimates.

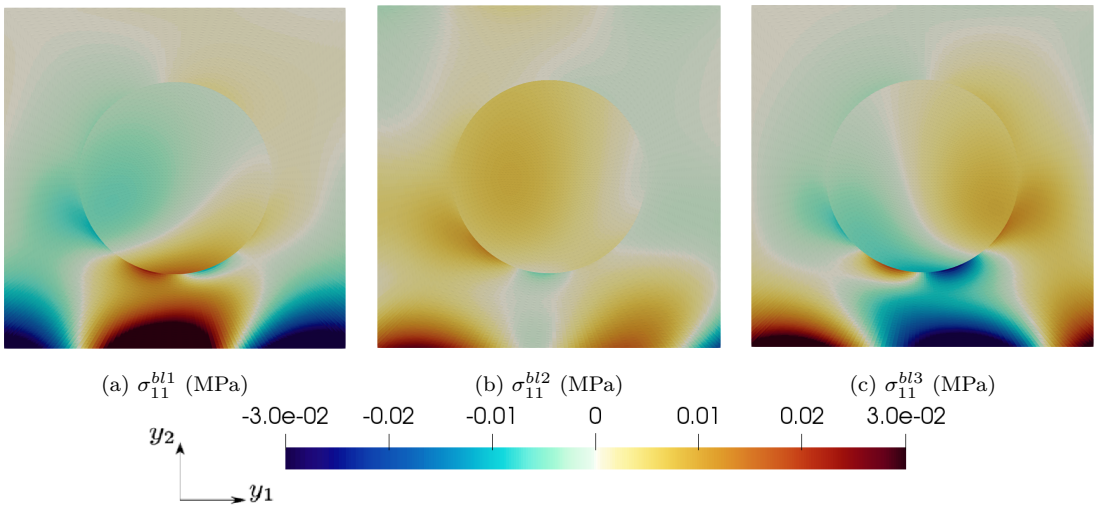

Figure 10: First (σ_{11}^{bl1}), second (σ_{11}^{bl2}), and third-order (σ_{11}^{bl3}) boundary layer correctors for the boundary cell with dashed line in Fig. 8. The decay inward (upper side of the unit-cell) of the corrections takes place over one unit-cell, but less pronounced for the second and third-order corrections.

Table 2: Comparison of the global relative modeling error for different fields.

Global modeling error	$k = est1$	$k = cor1$	$k = est2$	$k = cor2$	$k = est3$	$k = cor3$
$\frac{\|\boldsymbol{u}^{ref}-\boldsymbol{u}^{k}\|_{E(\Omega)}}{\|\boldsymbol{u}^{ref}\|_{E(\Omega)}}$	16.4%	12.7%	12.6%	6.1%	12.3%	5.1%

6. Conclusions

In this work, we have proposed a higher-order relocalization process, up to the third-order, to estimate heterogeneous fields without conducting DNS. The proposed relocalization introduces the effects of macroscale strain gradients, generally neglected by a classical first-order homogenization. As a result, the range of applicability of asymptotic homogenization/relocalization is extended to cases subjected to

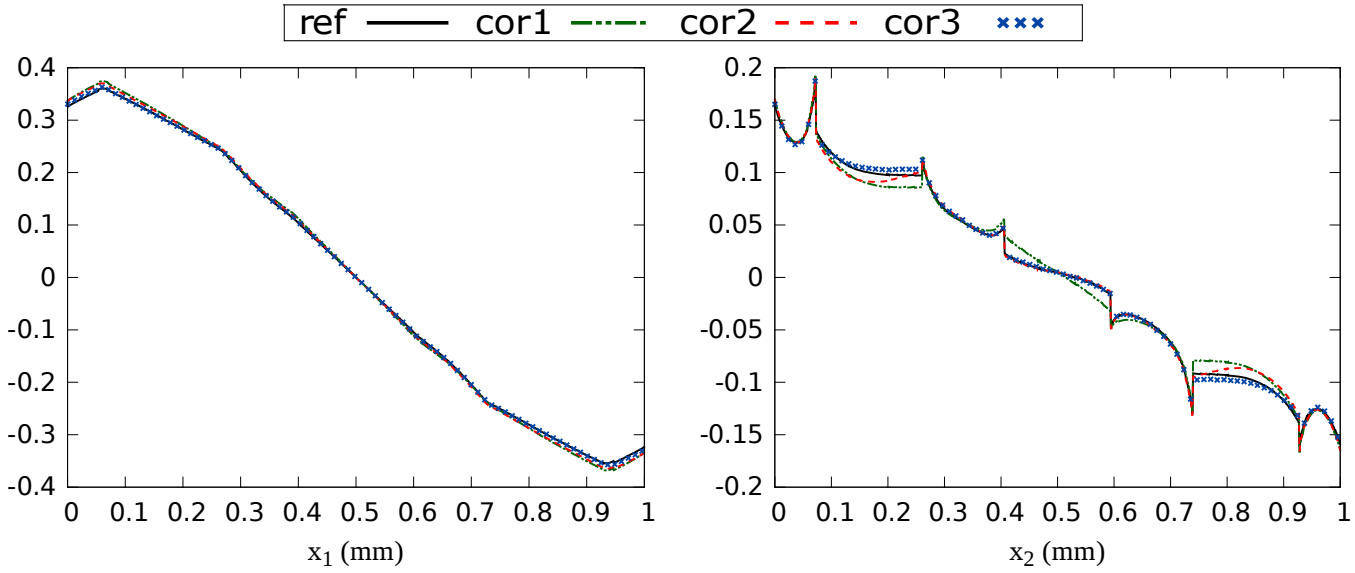

(a) σ_{11} (MPa) plotted along AB line

(b) σ_{12} (MPa) plotted along CD line

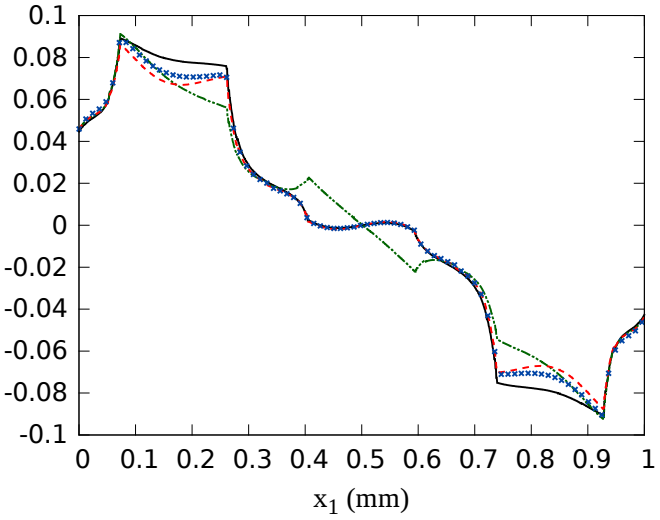

(c) σ_{11} (MPa) plotted along AB line

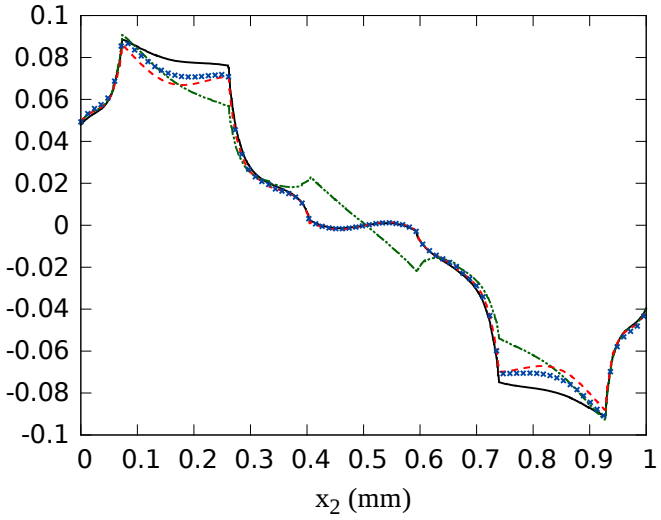

(d) σ_{12} (MPa) plotted along CD line

Figure 11: Results of the reference (ref) field compared with the first-order ($est1$), second-order ($est2$), and third-order ($est3$) estimates.

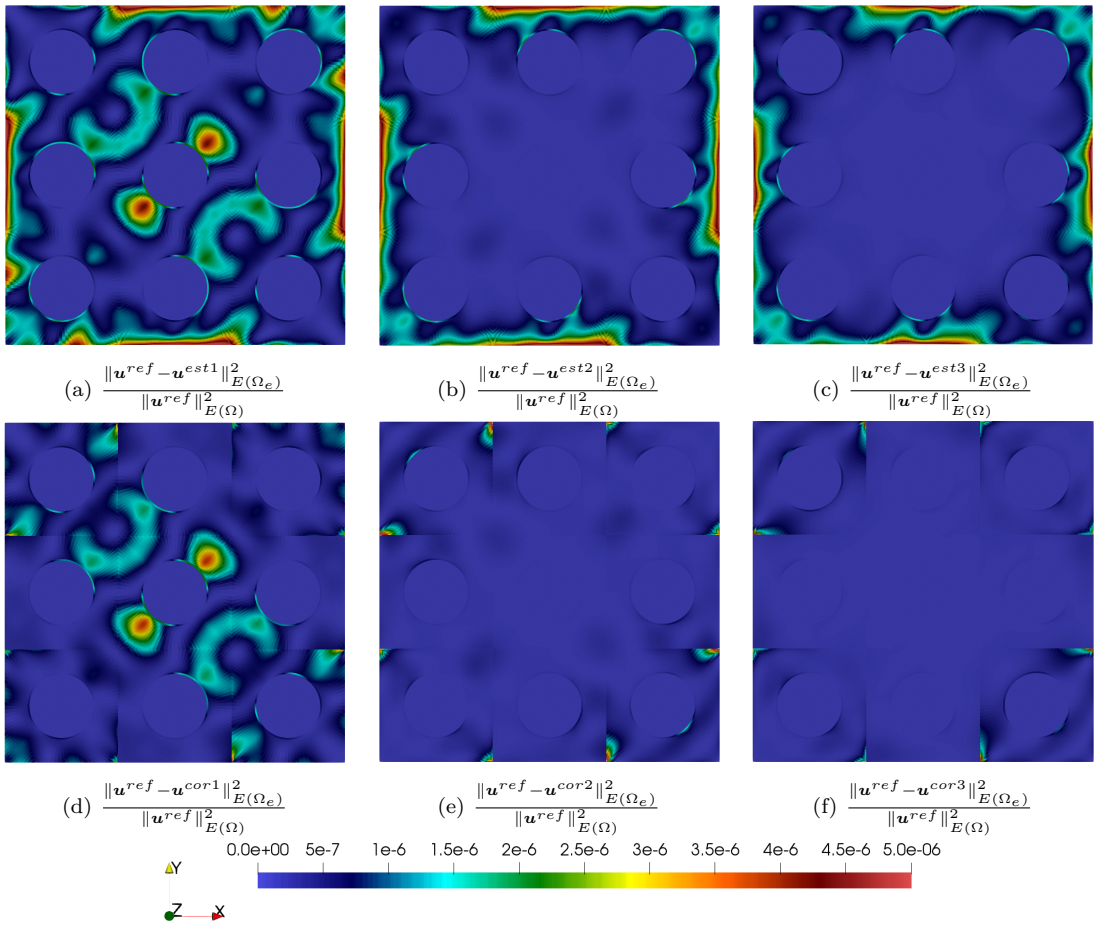

Figure 12: Comparison of the local relative modeling error results. The error is drastically reduced by increasing the order of the relocalization and boundary layer correction.

strong macroscale strain gradients. Our implementation of localization tensors has been verified, up to the third-order, based on analytical solutions provided by Boutin (1996). These tensors can be computed off-line and used for any composite structure involving the same unit-cell.

We have also proposed a general boundary layer correction based on asymptotic homogenization, up to the third-order, in order to estimate consistent microscale fields in the vicinity of the boundaries. The classical asymptotic homogenization is

modified at the boundaries by adding corrective terms, that decay toward the interior of the composite. These terms are obtained from the resolution of different problems over the unit-cell. The nature of the problems to be solved depends on the actual boundary conditions applied locally to the composite structure. The proposed boundary layer method is valid for different boundary conditions: Dirichlet, Neumann or mixed.

The major conclusions that can be drawn from this study are:

- The boundary layer correction decays within one unit-cell.
- First-order estimates may be inaccurate on the boundaries *and* in the inner domain of the structure. In contrast, second and third-order estimates are in good agreement with the reference fields inside the structure, but remain inaccurate at the boundaries.
- By increasing the order of the boundary layer correction, corrected fields progressively tend towards the reference.
- Higher-order relocalization combined with the boundary layer correction allows to drastically reduce the global modeling error by a factor of 3 to 4.
- Second and third-order corrected stress fields capture high stresses developed inside the structure *and* near boundary regions. In particular, for the laminated composite in bending shown in Sec. 5.1, σ_{12}^{est1} is 3 times smaller, inside the structure, than σ_{12}^{ref} and 5 times smaller near the sliding boundary. This may result in underestimating failure criteria if the design is conducted without the higher-order relocalization and boundary layer correction.

The proposed higher-order relocalization and boundary layer correction are applicable to 3D cases, but only 2D examples were provided for the sake of conciseness.

The suggested methods could be a path toward estimating microscale fields of 3D realistic engineering composite structures. This implies the use of irregular structure domains, coarse macroscale finite element meshes and locally nonperiodic zones.

Declaration of competing interest

The authors declare that they have no known competing financial interests or personal relationships that could have appeared to influence the work reported in this paper.

Acknowledgments

This work was supported by the French National Association for Research and Technology (ANRT) through the research grant CIFRE 2019/1715.

Appendix A: Numerical validation of localization tensors

The objective of this appendix is to validate our numerical implementation of higher-order localization tensors, up to the third-order. To do so, we compare the obtained numerical, relocalization and effective, tensors with their analytical solutions provided by Boutin (1996). For the sake of conciseness, expressions of analytical solutions are omitted.

A stratified composite is considered composed of two isotropic elastic layers a and b with respective thickness $(1-\tau)h$ and τh as shown in Fig. A.1a. The elastic moduli of the phase a and b are (E_a, ν_a) and (E_b, ν_b), respectively. Layers a and b are periodically distributed along the direction y_1, and remain unchanged by any translation along directions y_2 and y_3. Therefore, local fields depend only on variable y_1.

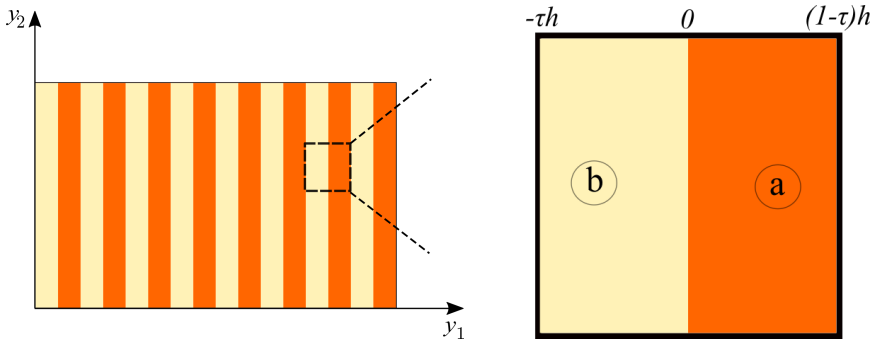

(a) Stratified composite geometry (b) Unit-cell domain

Figure A.1: Illustration of the studied problem.

For numerical simulations, the following material properties are considered: $E_b = 1\text{GPa}$, $E_a = 5\text{GPa}$ and $\mu_a = \mu_b = 0.3$ with $\tau = 0.5$.

First-order problem $\left(\mathcal{P}^{1^{st}}_{order}\right)$ *validation*

The solutions to these problems are first-order displacement, strain, and stress localization tensors: $\mathbb{D}^0$, $\mathbb{A}^0$, and $\mathbb{B}^0$, respectively.

Components D^0_{111} and A^0_{1111} are shown in Fig. A.2a and A.2b, respectively. Displacement fields, *i.e.* components of $\mathbb{D}^0$, are piecewise linear as shown in Fig. A.2c while strain fields, *i.e.* components of $\mathbb{A}^0$, are constant per layer as shown in Fig. A.2d. Comparison between obtained numerical and analytical solutions of first-order displacement, strain, and stress localization tensors: $\mathbb{D}^0$, $\mathbb{A}^0$, and $\mathbb{B}^0$ are shown in figures A.2c, A.2d and A.2e, which are in perfect agreement.

Remark A.1. *By a volume average process on* $\mathbb{B}^0$*, one can deduce the homogenized elasticity tensor* $\mathbb{C}^0$*. An orthotropic macroscopic elastic behavior is obtained.*

Second-order problem $\left(\mathcal{P}^{2^{nd}}_{order}\right)$ *validation*

The solutions to these problems are second-order displacement, strain, and stress localization tensors: $\mathbb{D}^1$, $\mathbb{A}^1$, and $\mathbb{B}^1$, respectively.

Components D^1_{2222} and A^1_{12222} are shown in figures A.2a and A.2b, respectively. Displacement fields are now quadratic functions as shown in Fig. A.3c while strain fields are piecwise linear as shown in Fig. A.3d. Comparison between obtained numerical and analytical solutions of second-order displacement, strain, and stress localization tensors: $\mathbb{D}^1$, $\mathbb{A}^1$, and $\mathbb{B}^1$ are shown in figures A.3c, A.3d and A.3e, which are in perfect agreement.

Remark A.2. *Components of* $\mathbb{B}^1$ *have a zero volume average on the unit-cell. Therefore, the second-order effective tensor* $\mathbb{C}^1 = 0$*, which is a fifth-rank tensor.*

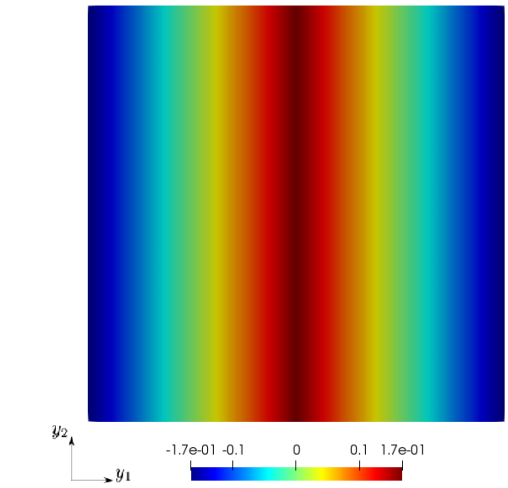

(a) D^0_{111} component

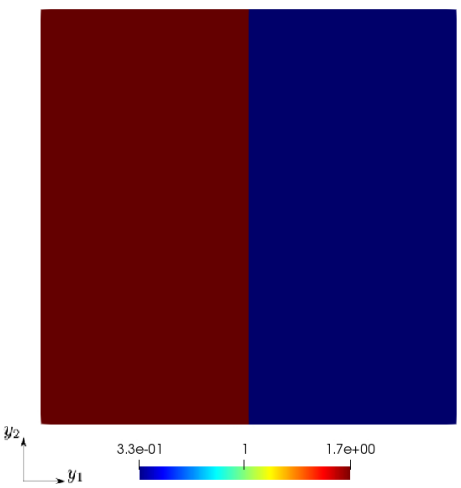

(b) A^0_{1111} component

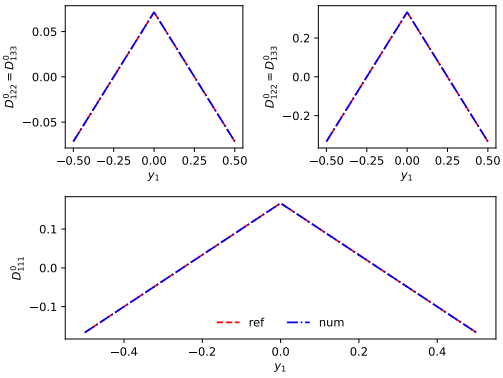

(c) Non-zero components of $\mathbb{D}^0$

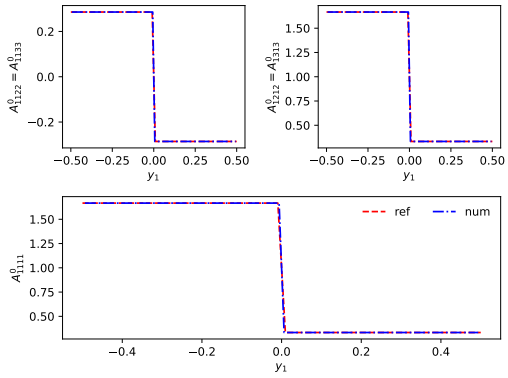

(d) Non-zero components of $\mathbb{A}^0$

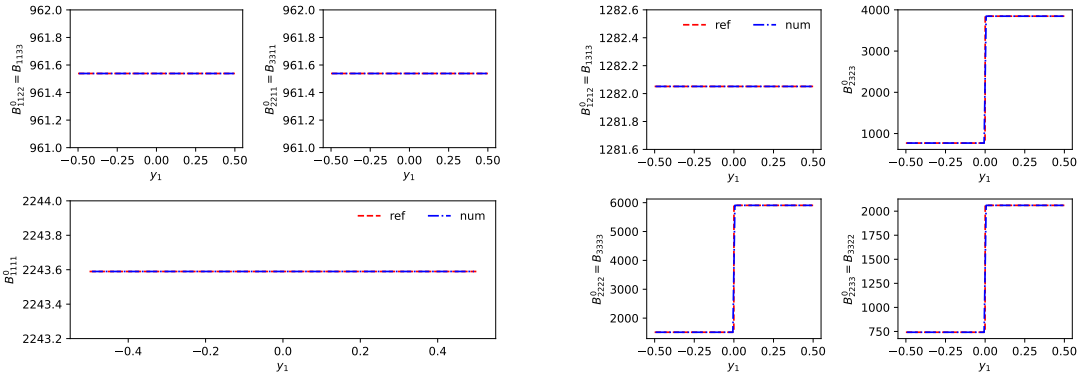

(e) Non-zero components of $\mathbb{B}^0$

Figure A.2: Results of the first-order homogenization problem $\left(\mathcal{P}^{1^{st}}_{order}\right)$. Figures A.2c, A.2d and A.2e show perfect agreement between numerical (in blue) and analytical (in red) results.

Third-order problem $\left(\mathcal{P}^{3^{rd}}_{order}\right)$ *validation*

The solutions to these problems are third-order displacement, strain, and stress localization tensors: $\mathbb{D}^2$, $\mathbb{A}^2$, and $\mathbb{B}^2$, respectively.
Components (D^2_{12222}, B^2_{222222}) and (D^2_{21121}, A^2_{121121}) are shown in Fig. A.4. Displacement fields are now cubic functions as shown in figures A.4b and A.4f while stress/strain fields are quadratic functions as shown in figures A.4d and A.4h.

Remark A.3. *After averaging values of* $\mathbb{B}^2$*, one can deduce the third-order effective tensor* $\mathbb{C}^2$*, which is a sixth-rank tensor. Analytical expression of* $\mathbb{D}^2$*,* $\mathbb{A}^2$*, and* $\mathbb{B}^2$ *were not provided in Boutin (1996), but values of* $\mathbb{C}^2$ *are detailed. We have verified that we obtain,* ***exactly****, the same values of* $\mathbb{C}^2$ *provided in Boutin (1996) by our numerical procedure.*

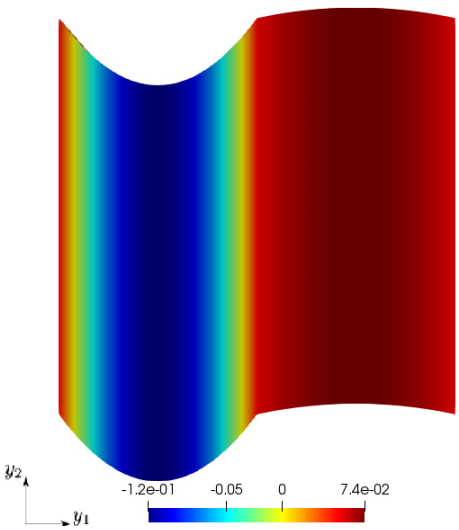

(a) D^1_{2222} component
(magnification of 10)

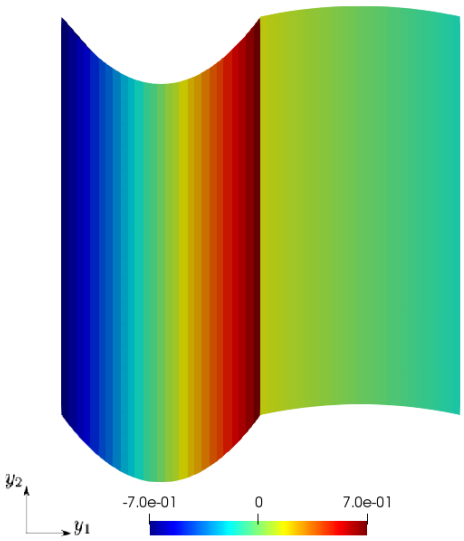

(b) A^1_{12222} component
(magnification of 10)

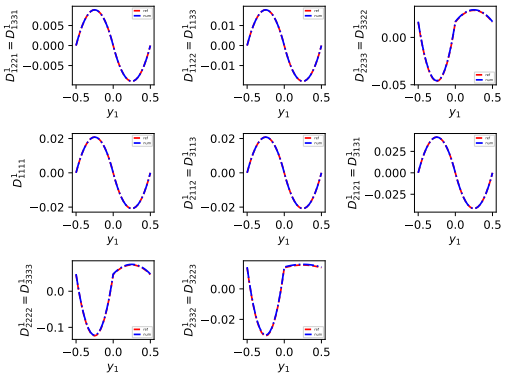

(c) Non-zero components of $\mathbb{D}^1$

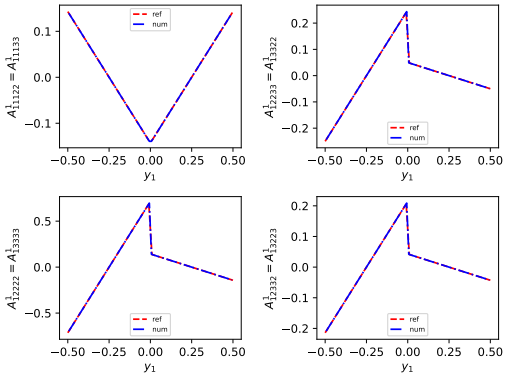

(d) Non-zero components of $\mathbb{A}^1$

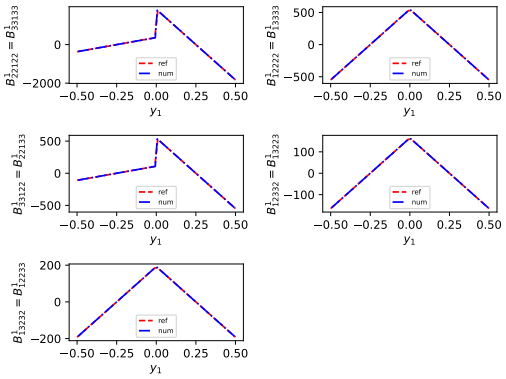

(e) Non-zero components of $\mathbb{B}^1$

Figure A.3: Results of the second-order homogenization problem $\left(\mathcal{P}^{2^{nd}}_{order}\right)$. Figures A.3c, A.3d and A.3e show perfect agreement between numerical (in blue) and analytical (in red) results.

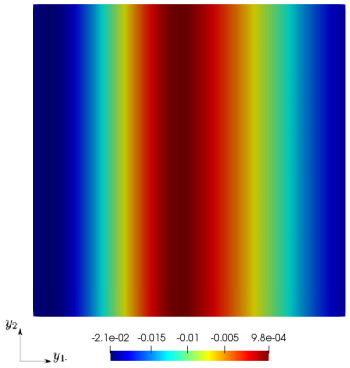

(a) D^2_{12222} component

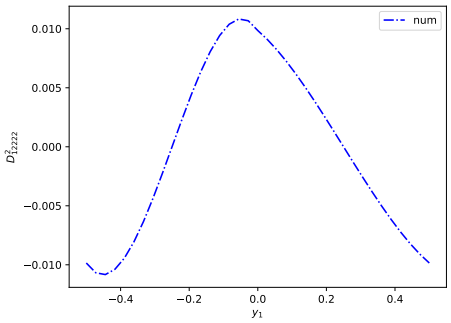

(b) D^2_{12222} values along y_1

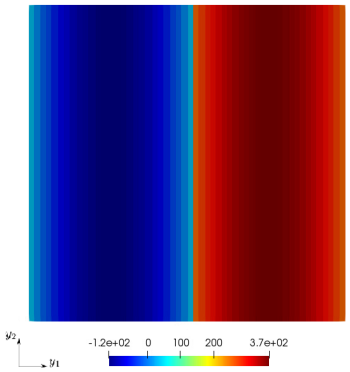

(c) B^2_{222222} component

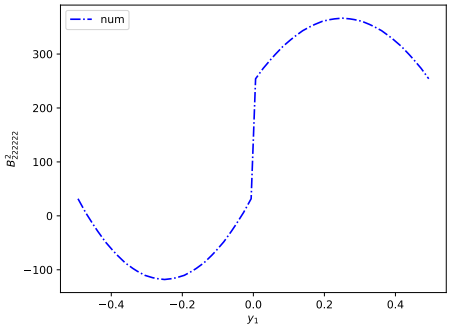

(d) B^2_{222222} values along y_1

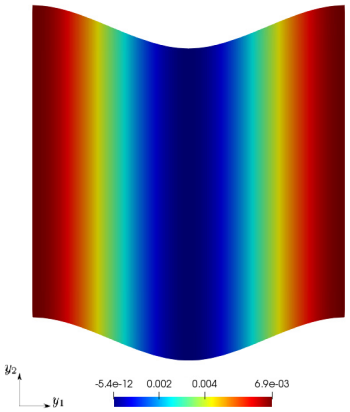

(e) D^2_{21121} component
(magnification of 20)

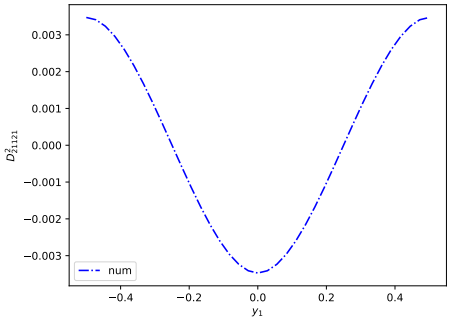

(f) D^2_{21121} values along y_1

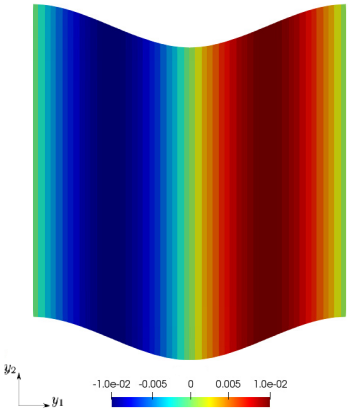

(g) A^2_{121121} component
(magnification of 10)

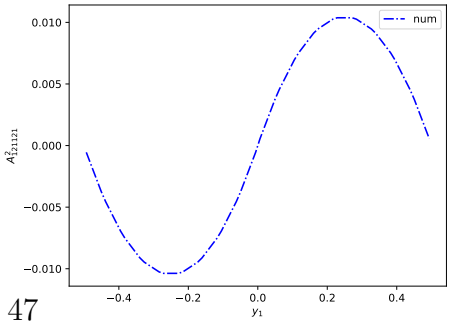

(h) A^2_{121121} values along y_1

Figure A.4: Third-order relocalization components (D^2_{12222}, B^2_{222222}) and (D^2_{21121}, A^2_{121121}).

Appendix B: Comparative study

The objective of this appendix is to compare our results of higher-order relocalization and boundary layer correction with those obtained in He and Pindera (2020a). First, second and third-order components of stress localization tensors are shown in Fig. B.1. These results are to be compared with those presented in He and Pindera (2020a) (see their figure 3), where a finite-volume method was used to compute localization tensors. It is noticed that exactly the same results are obtained.

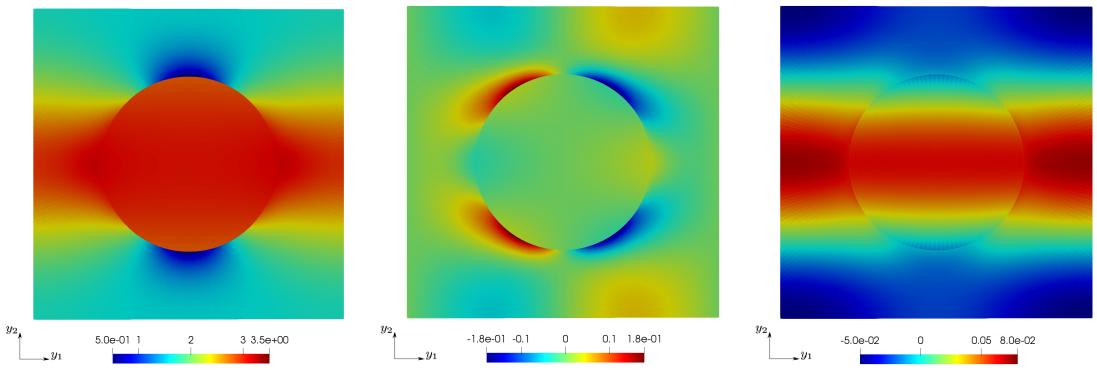

(a) B^0_{1111} (MPa) (b) B^1_{11111} (MPa) (c) B^2_{111111} (MPa)

Figure B.1: First, second and third-order components of stress localization tensors produced by a *unit* loadings.

Remark B.1. *The component B^1_{11111} has a zero average distribution over the unit-cell, implying that the first component of the second-order effective tensor $C^1_{11111} = 0$. In general, $\mathbb{C}^1 = 0$ in case of centro-symmetric unit-cell.*

Comparison of different stress fields σ_{11} are shown in Fig. B.2. By increasing the order of the relocalization, estimated stress fields approach progressively the reference. Figures B.2e and B.2f show that a third-order relocalization provides a good estimation in the inner domain of the structure, nevertheless accuracy is lost near the

boundaries. Similar results are shown in He and Pindera (2020a) (see their figure 5).

Comparison of stress fields, after the boundary layer correction, are shown in

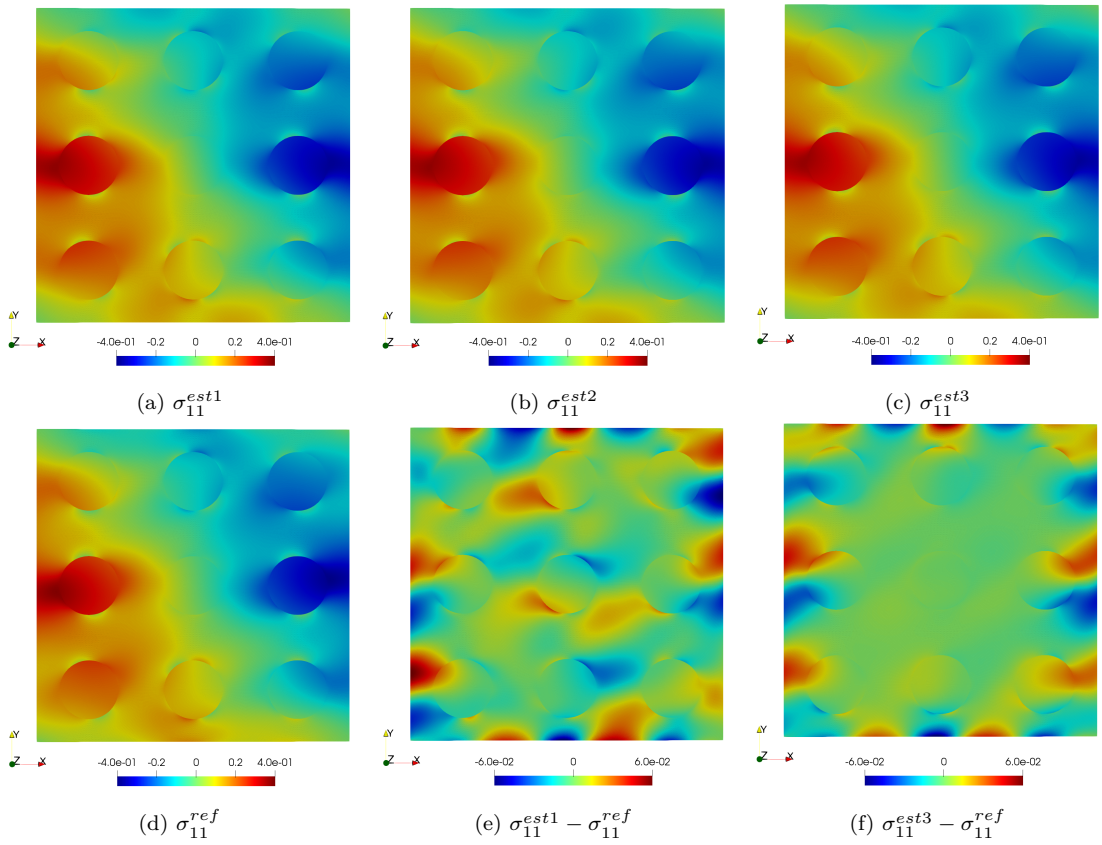

(a) σ_{11}^{est1} (b) σ_{11}^{est2} (c) σ_{11}^{est3}

(d) σ_{11}^{ref} (e) $\sigma_{11}^{est1} - \sigma_{11}^{ref}$ (f) $\sigma_{11}^{est3} - \sigma_{11}^{ref}$

Figure B.2: Comparison of different stress fields σ_{11} (MPa). By increasing the order of the relocalization, estimated stress fields approach progressively the reference, yet remain inaccurate near the boundaries.

Fig. B.3. It is noticed that the corrected stress, σ_{11}^{cor3}, provides a better estimation near the boundaries (see figure B.3b), contrary to σ_{11}^{est3} in figure B.2f.

In He and Pindera (2020a), a boundary layer correction is conducted by applying the third-order relocalized displacement field in the inner domain of the *fully* detailed, *i.e.* using DNS, boundary.

By comparing our results, it is noticed that a better approximation of σ_{11}^{cor3} is provided by the boundary correction by He and Pindera (2020a), albeit at a higher computing cost. Indeed, instead of conducting DNS, which may be computationally cumbersome when the boundary domain is large, our method introduce corrective terms computed on a *single unit-cell*.

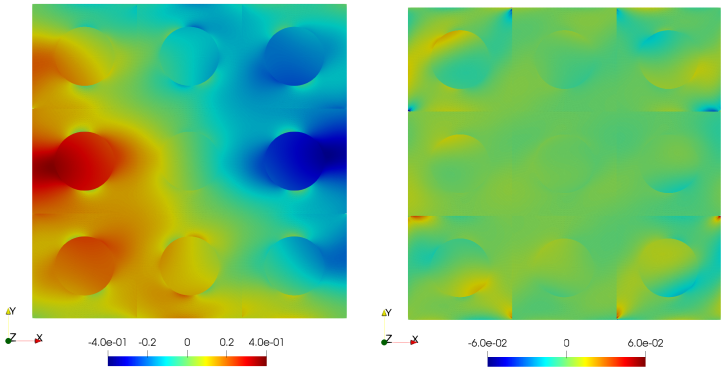

(a) σ_{11}^{cor3} (b) $\sigma_{11}^{cor3} - \sigma_{11}^{ref}$

Figure B.3: Comparison of corrected stress fields σ_{11} (MPa). σ_{11}^{cor3} provides a better approximation than σ_{11}^{est3} as shown in Fig. B.2f.

Appendix C: Limitation of the proposed approach

We consider a plane strain elasticity problem of a laminated composite made of two layers as presented in Fig. C.1. The size of the structure is $L = 8$ mm, $H = 5$ mm and $W = 1$ mm. The two layers are assumed to be isotropic linear elastic with coefficients ($E_f/E_m = 200$, $\nu_m = \nu_f = 0.3$). The structure is fixed on the left whereas a prescribed displacement $u_2 = -2$ mm is applied on the right, as shown in Fig. C.1.

The comparison between the reference displacement field u_2^{ref} and the homogenized

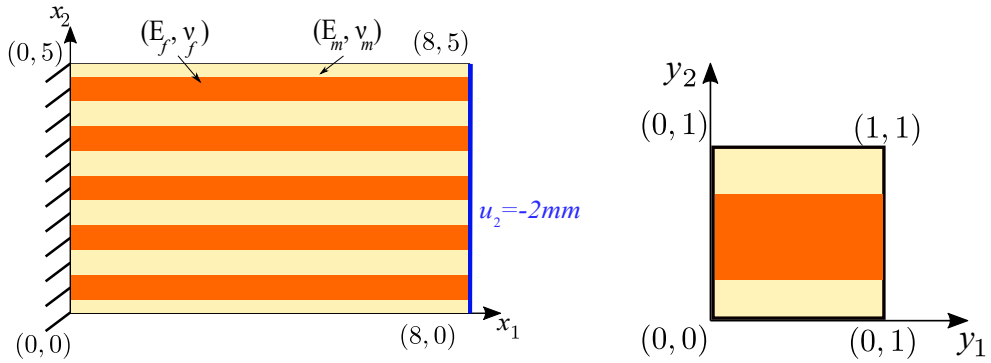

(a) Structure geometry (b) Unit-cell domain

Figure C.1: Illustration of a laminated composite in bending. The structure is fixed on the left, a displacement $u_2 = -2$ mm is applied on the right.

one u_2^{hom}, using conventional Cauchy continuum, are presented in Fig. C.2. It can be seen that the Cauchy medium gives a poor prediction of the real deformation state. This is due to the fact that it is not able to take into account the clamping conditions. Consequently, the relocalization process will be inaccurate, even including higher-order terms, since the resulting macroscale strain and its gradients, considering a Cauchy continuum, are inaccurate and not representative of the deformation state, especially near the fixed boundary, which can be seen in Fig. C.3. Cosserat

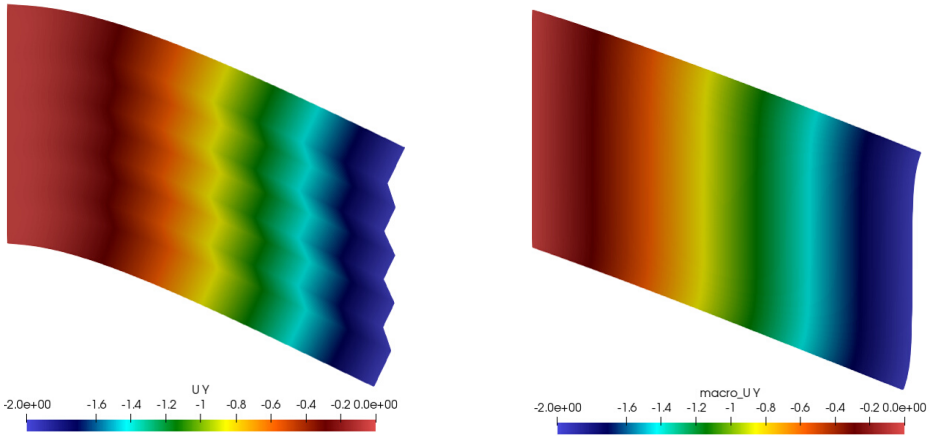

(a) u_2^{ref} (b) u_2^{hom}

Figure C.2: Comparison between the reference and homogenized displacement field u_2.

medium was considered at the macroscale in Forest and Sab (1998) providing better solutions. A higher-order relocalization, using a Cosserat medium at the macroscale, is supposed then to provide better solutions than those presented in Fig. C.3. A macroscopic strain gradient approach would also provide a better solution.

Remark C.1. *When considering a structure constructed by one of the two unit-cells presented in subsection 5.1 or 5.2 and subjected to the same boundary conditions in Fig. C.1a, the macroscale strain and its gradients, using a Cauchy continuum, will be representative of the deformation state. Consequently, higher-order estimates will accurately approximate reference fields. The need of a higher-gradient continuum is, therefore, specific to both the considered microstructure and loading conditions.*

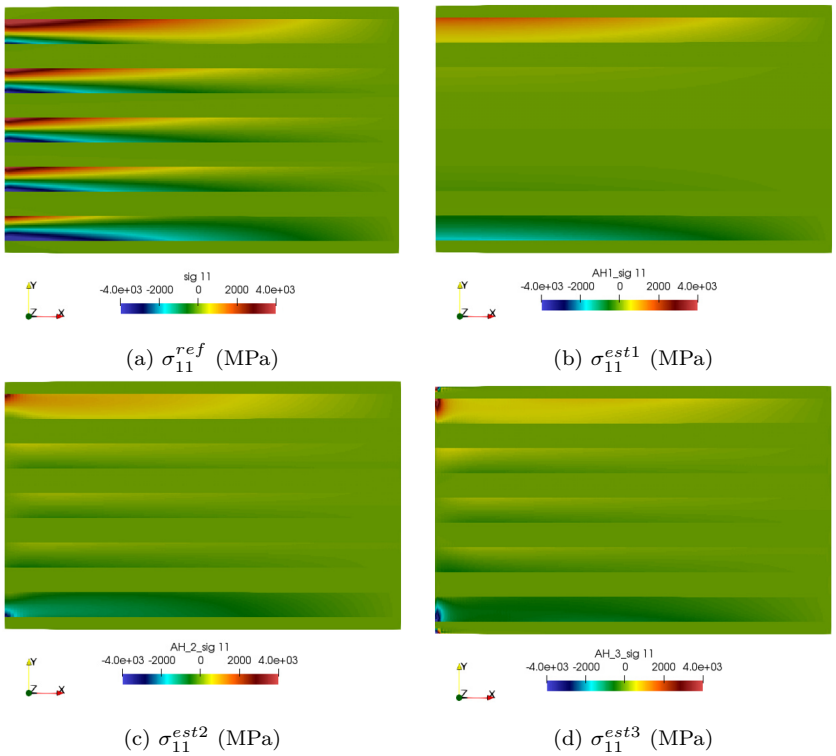

(a) σ_{11}^{ref} (MPa)

(b) σ_{11}^{est1} (MPa)

(c) σ_{11}^{est2} (MPa)

(d) σ_{11}^{est3} (MPa)

Figure C.3: Results of the reference (σ_{11}^{ref}) field compared with the first-order (σ_{11}^{est1}), second-order (σ_{11}^{est2}), and third-order (σ_{11}^{est3}) estimates for the laminated composite in bending.

References

Ameen, M., Peerlings, R., Geers, M., 2018. A quantitative assessment of the scale separation limits of classical and higher-order asymptotic homogenization. European Journal of Mechanics - A/Solids 71, 89–100.

Auffray, N., Dirrenberger, J., Rosi, G., 2015. A complete description of bi-dimensional anisotropic strain-gradient elasticity. International Journal of Solids and Structures 69, 195–206.

Bensoussan, A., Lions, J.L., Papanicolaou, G., 2011. Asymptotic analysis for periodic structures. volume 374. American Mathematical Soc.

Boutin, C., 1996. Microstructural effects in elastic composites. International Journal of Solids and Structures 33, 1023–1051.

Cosserat, E., Cosserat, F., 1909. Theorie des corps déformables. A. Hermann et fils.

Dumontet, H., 1986. Study of a boundary layer problem in elastic composite materials. ESAIM: Mathematical Modelling and Numerical Analysis 20, 265–286.

Fergoug, M., Parret-Fréaud, A., Feld, N., Marchand, B., Forest, S., 2022. A general boundary layer corrector for the asymptotic homogenization of elastic linear composite structures. Composite Structures 285, 115091.

Forest, S., 1998. Mechanics of generalized continua: construction by homogenization. Le Journal de Physique IV 8, Pr4–39.

Forest, S., Pradel, F., Sab, K., 2001. Asymptotic analysis of heterogeneous Cosserat media. International Journal of Solids and Structures 38, 4585–4608.

Forest, S., Sab, K., 1998. Cosserat overall modeling of heterogeneous materials. Mechanics research communications 25, 449–454.

Forest, S., Trinh, D., 2011. Generalized continua and non-homogeneous boundary conditions in homogenisation methods. ZAMM - Journal of Applied Mathematics and Mechanics / Zeitschrift für Angewandte Mathematik und Mechanik 91, 90–109.

Germain, P., 1973. The method of virtual power in continuum mechanics. part 2: Microstructure. SIAM Journal on Applied Mathematics 25, 556–575.

Gologanu, M., Leblond, J.B., Perrin, G., Devaux, J., 1997. Recent extensions of Gurson's model for porous ductile metals, in: Continuum micromechanics. Springer, pp. 61–130.

He, Z., Pindera, M.J., 2020a. Finite volume-based asymptotic homogenization of periodic materials under in-plane loading. Journal of Applied Mechanics 87, 121010.

He, Z., Pindera, M.J., 2020b. Locally exact asymptotic homogenization of periodic materials under anti-plane shear loading. European Journal of Mechanics - A/Solids 81, 103972.

Hsu, P.W., Herakovich, C.T., 1977. Edge effects in angle-ply composite laminates. Journal of Composite Materials 11, 422–428.

Huet, C., 1990. Application of variational concepts to size effects in elastic heterogeneous bodies. Journal of the Mechanics and Physics of Solids 38, 813–841.

Kanit, T., Forest, S., Galliet, I., Mounoury, V., Jeulin, D., 2003. Determination of the size of the representative volume element for random composites: statistical and numerical approach. International Journal of solids and structures 40, 3647–3679.

Koley, S., Mohite, P., Upadhyay, C., 2019. Boundary layer effect at the edge of fibrous composites using homogenization theory. Composites Part B: Engineering 173, 106815.

Kouznetsova, V., Geers, M.G., Brekelmans, W.M., 2002. Multi-scale constitutive modelling of heterogeneous materials with a gradient-enhanced computational homogenization scheme. International Journal for Numerical Methods in Engineering 54, 1235–1260.

Kruch, S., 2007. Homogenized and relocalized mechanical fields. The Journal of Strain Analysis for Engineering Design 42, 215–226.

Kruch, S., Forest, S., 1998. Computation of coarse grain structures using a homogeneous equivalent medium. Journal de Physique IV 08, Pr8–197–Pr8–205.

Mindlin, R.D., 1964. Micro-structure in linear elasticity. Archive for Rational Mechanics and Analysis 16, 51–78.

Mindlin, R.D., Eshel, N., 1968. On first strain-gradient theories in linear elasticity. International Journal of Solids and Structures 4, 109–124.

Monchiet, V., Auffray, N., Yvonnet, J., 2020. Strain-gradient homogenization: A bridge between the asymptotic expansion and quadratic boundary condition methods. Mechanics of Materials 143, 103309.

Pagano, N.J., 1978. Free edge stress fields in composite laminates. International Journal of Solids and Structures 14, 401–406.

Peerlings, R.H.J., Fleck, N.A., 2004. Computational Evaluation of Strain Gradient Elasticity Constants. International Journal for Multiscale Computational Engineering 2, 599–620.

Pipes, R.B., Kaminski, B., Pagano, N., 1973. Influence of the free edge upon the strength of angle-ply laminates, in: Analysis of the test methods for high modulus fibers and composites. ASTM International.

Sanchez-Palencia, E., 1983. Homogenization method for the study of composite media, in: Asymptotic Analysis II—. Springer, pp. 192–214.

Sanchez-Palencia, E., 1986. Homogenization in mechanics. a survey of solved and open problems. Rend. Sem. Mat. Univ. Politec. Torino 44, 1–45.

Sanchez-Palencia, E., Zaoui, A., 1987. Homogenization techniques for composite media. Homogenization techniques for composite media 272.

Smyshlyaev, V.P., Cherednichenko, K.D., 2000. On rigorous derivation of strain gradient effects in the overall behaviour of periodic heterogeneous media. Journal of the Mechanics and Physics of Solids 48, 1325–1357.

Suquet, P., 2014. Continuum micromechanics. volume 377. Springer.

Tang, S., Levy, A., 1975. A boundary layer theory-part ii: extension of laminated finite strip. Journal of Composite Materials 9, 42–52.

Tran, T.H., Monchiet, V., Bonnet, G., 2012. A micromechanics-based approach for the derivation of constitutive elastic coefficients of strain-gradient media. International Journal of Solids and Structures 49, 783–792.

Yuan, X., Tomita, Y., Andou, T., 2008. A micromechanical approach of nonlocal modeling for media with periodic microstructures. Mechanics Research Communications 35, 126–133.

Yvonnet, J., Auffray, N., Monchiet, V., 2020. Computational second-order homogenization of materials with effective anisotropic strain-gradient behavior. International Journal of Solids and Structures 191-192, 434–448.